IEEE Open Journal of Engineering in Medicine and Biology

Emerging Topics

Printed Strain Sensors for Motion Recognition: A Review of Materials, Fabrication Methods, and Machine Learning Algorithms

Nathan Zavanelli[1,2]†, Kangkyu Kwon[2,3]†, and Woon-Hong Yeo[1,2,4,5*], *Senior Member, IEEE*

***Abstract*— Recent studies in functional nanomaterials with advanced macro, micro, and nano-scale structures have yielded substantial improvements in human-interfaced strain sensors for motion and gesture recognition. Furthermore, fundamental advances in nanomaterial printing have been developed and leveraged to translate these materials and mechanical innovations into practical applications. Significant progress in machine learning for human-interfaced strain sensing has unlocked numerous opportunities to improve lives and the human experience through healthcare innovations, sports performance monitoring, and human-machine interfaces. However, several key challenges still must be overcome if strain sensors are to become ubiquitous tools for human motion recognition. This review begins with a summary of the critical strain-sensing mechanisms employed today and how recent works have sought to push their boundaries. It then proceeds to cover the primary functional materials used in wearable strain sensors from a performance and printability perspective. Next is a review of recent advances in nanomaterial printing to produce the complex structures necessary for functional devices. Next, we summarize machine learning approaches for human gesture recognition and the myriad applications and use cases for human-interfaced strain sensors. Finally, it concludes with a discussion of challenges and opportunities for future research in the field.**

***Index Terms* – strain sensor, printed electronics, wearables, machine learning, motion recognition**

***Impact Statement* – This review summarizes the key advances in materials, fabrication methods, and machine learning algorithms that are driving exciting progress in human motion recognition based on skin-interfaced strain sensors.**

[1]George W. Woodruff School of Mechanical Engineering, Georgia Institute of Technology, Atlanta, GA 30332
[2]IEN Center for Human-Centric Interfaces and Engineering, Institute for Electronics and Nanotechnology, Georgia Institute of Technology, Atlanta, GA, 30332
[3]School of Electrical and Computer Engineering, Georgia Institute of Technology, Atlanta, GA 30332
[4]Wallace H. Coulter Department of Biomedical Engineering, Georgia Institute of Technology and Emory University School of Medicine, Atlanta, GA 30332
[5]Parker H. Petit Institute for Bioengineering and Biosciences, Neural Engineering Center, Institute for Materials, Institute for Robotics and Intelligent Machines, Georgia Institute of Technology, Atlanta, GA 30332
†These authors equally contributed to this work
*Corresponding author email: whyeo@gatech.edu

I. Introduction

Strain sensors encompass a broad class of devices that transduce mechanical deformations and strains into an electrical signal. When attached to the skin, their ability to precisely characterize skin deformations makes them an ideal sensor for human motion and gesture recognition[1-5]. These sensors may be judiciously placed around key joints and analyzed with machine learning algorithms for many diverse applications, including human machine interfaces, rehabilitation, and healthcare[6-14]. For these systems to be effective and scalable for clinical and commercial use, several key requirements must be met. First, the strain sensors must well match the mechanical properties of the skin, allowing them to seamlessly stretch and flex during skin deformations[15]. They should have a low elastic modulus, the epidermis and dermis have elastic moduli of 140-600 kPa and 2-80 kPa, respectively, and stretchability suited for the region of interest, which can range from 10-80%[16]. The requirements for a low elastic modulus and high stretchability are typically achieved by integrating a very thin (< 20 μm) metal, conductive polymer composite, or conductive nanomaterial dispersion in a stretchable substrate, like urethane or fabric[17-19]. Second, the sensors must be highly sensitive over the strain region of interest, which is controlled primarily by the material properties and judicious patterning of the sensor[11, 20, 21]. Third, they must be durable over repeated uses[16]. This is determined by the mechanical strength of the materials used and the method of integration[22, 23]. Fourth, they must be biocompatible, which is again controlled by the materials and integration strategy[24, 25]. The final key requirement for the physical sensors is that they may be rapidly manufactured in a scalable fabrication process[26, 27]. For instance, photolithographic patterning and complex two stage transfer fabrication has yielded exceptional strain gauge performance, but such approaches are not suited for industrial scales[4, 17]. Instead, fully printed sensors, which in many cases may be integrated into mature roll to roll manufacturing systems, offer a much more attractive method to translate fundamental discoveries in materials and interfaces for strain sensors to practical applications[27, 28]. A summary of these key requirements is shown in Figure 1.

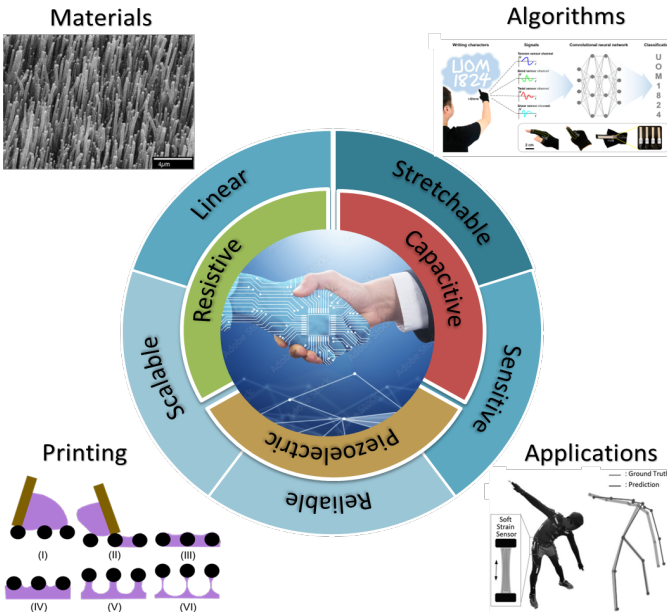

Figure 1. Overview of printed strain sensors for motion recognition. Top left reprinted with permission from Appl Phys Lett 73(26):3845 – 3847. Bottom left reprinted with permission from ACS Omega (2021) 6, 14, 9344–9351. Top right reprinted under Creative Commons license CC BY 4.0 from Spring Nature. Bottom right reprinted from IEEE Access, copyright ©[2019] IEEE.

A variety of materials and fabrication techniques have been proposed to develop human interfaced strain sensors, but the most promising for scalable systems involve directly printing a functional sensing material on a stretchable substrate[29-34]. In these approaches, a conductive nanomaterial or polymer is typically dispersed in a printable ink, which is then deposited using either contact or non-contact printing methods[33-36]. Recent advances in printable nanoparticle, nanowire, nanotube, polymer, and piezoelectric crystal dispersions for strain sensors have greatly improved sensor performance and unlocked novel applications in human motion recognition[4, 37]. These materials may be printed with contact methods, like screen, gravure, and flexographic printing, or non-contact methods, like inkjet, aerosol jet, and electrohydrodynamic (EHD) printing[33, 34, 38-40]. The advantages and limitations of each method will be discussed in depth in section 4. Compared to traditional microfabrication approaches, all these methods offer much lower material waste, lower cost, higher throughput, and simpler integration, making them highly attractive for practical strain sensing applications[33].

Finally, the sensors must be integrated into a functional system with wearable electronics capable of either detecting motion on-site or broadcasting data to a remote processor via Bluetooth[4]. These systems often must be minimally obtrusive to the user and highly portable, requiring them to either utilize skin-interfaced electronics or electronic garments[17, 18]. Furthermore, machine learning algorithms must be developed and tuned to classify human motions based on the sensor data[6, 41].

The purpose of this review is to summarize the key advances in materials, fabrication methods, and machine learning algorithms that are driving exciting progress in human motion recognition based on skin-interfaced strain sensors. The review is organized into the following sections: First, Section 2 summarizes the three primary sensing mechanisms employed for these devices. In Section 3, the most promising materials for strain sensors are surveyed, with a focus on their performance and manufacturing tradeoffs. Section 4 details the various printing methods currently under investigation, with a similar focus on material ink requirements, manufacturing scalability and patterning control. Next, Section 5 presents several machine learning approaches for human motion recognition based on wearable strain sensor networks. Applications based on these fully integrated systems are then explored in Section 6, and the review concludes with a perspective on the crucial challenges and future direction of the field in Section 7.

II. Strain Sensor Operating Principles

Strain gauges utilize the unique material properties of an active sensing material to transduce mechanical strain into an electrical signal. In printed strain gauges, this is usually achieved through resistive, capacitive, or piezoelectric effects. Although traditional strain gauges have relied primarily on purely geometric changes to elicit these three effects, novel sensors are being developed that incorporate various disconnection, crack propagation, tunnelling, and percolation threshold phenomena to increase sensor resistivity. In each method, the specific material properties and microstructures, pattern thickness and geometry, material loading, substrate choice, and post-print processing play crucial roles in determining sensor performance. Understanding these key parameters will be the focus of sections 3 and 4 of this review; first, however, section 3 will briefly detail the three primary strain transduction mechanisms used in printed, human-interfaced strain sensors, and these approaches are furthermore characterized in Table 1 and illustrated in Figure 2.

A. Resistive Strain Sensors

The most common resistive strain transduction mechanism, and indeed the most ubiquitous of all three approaches, utilizes the piezoresistive effect[24, 42-46]. Quite simply, the electrical resistance of a material changes according to Ohm's Law based on the following relationship:

$$R = \rho \frac{l}{A}$$

where ρ is the electrical resistivity, A is the cross-sectional area A, and l is the material length. When a material is stretched, the length and cross-sectional area change in accordance with the material's Poisson ratio ν:

$$\nu = \frac{-d\varepsilon_{trans}}{d\varepsilon_{axial}}$$

where ε_{trans} is the transverse strain and ε_{axial} is the axial strain. This geometric alteration based on the Poisson ratio alone, however, induces a relatively small gauge factor, which is defined as the change in resistance with strain. The sensor's gauge factor, and thus sensitivity, can be greatly improved by also incorporating strain dependent changes in resistivity. Thus, the gauge factor based purely on intrinsic material properties can be defined as:

$$GF_{piezoresistive} = \frac{\Delta R/R}{\varepsilon} = 1 + 2\nu + \frac{\Delta\rho/\rho}{\varepsilon}$$

where ε is the applied strain. Whereas traditional strain sensors rely solely on these intrinsic material properties, advanced sensors can achieve improved gauge factors by inducing microstructural changes that affect conductive pathways[25, 47-53]. One of the most common methods is by embedding the conductive nanomaterials in a polymer matrix with a loading percentage near the percolation threshold, which is the minimum material loading needed to form a highly conductive network[42, 54, 55]. Thus, any small changes in the material contacts will yield high changes in resistance. For instance, embedded silver nanowires (NWs) were embedded in a PDMS matrix with an optimized material loading such that conductivity is maintained, but greatly reduced with strain[56]. Although this method is achievable with all nanomaterials, it is best suited to those with high aspect ratios, like NWs and nanotubes (NTs) because they can best avoid total disconnections because of their long lengths[42, 54, 55].

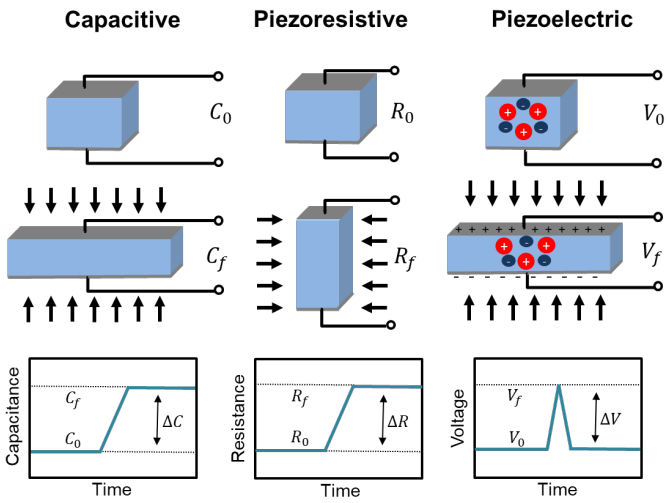

Figure 2. Illustrations of the three primary approaches to strain sensing in human interfaced electronics. C_0, R_0, and V_0 represent the initial capacitance, resistance, and voltage, respectively, while C_f, R_f, and V_f represent the final capacitance, resistance, and voltage, respectively. The plots in the lower portion of the figure represent the response to an impulse strain.

In addition to causing disconnections at the nano-scale, microscale disconnections may be induced through a cracking method[57-59]. Typically, a thin metal is deposited on a polymer or fiber substrate, and micro-cracks are induced because of the mismatch in material moduli. For instance, an Ag ink was printed over a silicone elastomer and used a cracking mechanism to observe excellent gauge factors of over 1000 with up to 75% strain[60]. One key limitation of this approach, however, is that these cracks do not self-heal after strain, leading to a reduced gauge factor after repeated uses. This limitation can be circumvented by using a simple disconnection instead of a full crack, although this approach tends to exhibit a lower gauge factor[11, 28, 52, 61, 62]. As an example, one group used a buckling disconnection mechanism to achieve high stretchability (300%) and an acceptable gauge factor of 48[63]. In addition, the quantum tunneling effect can be used to yield an improved gauge factor. In this mechanism, charges may penetrate an energy barrier based on the probability density of the charge carrier, and the tunneling resistance depends on the tunnel barrier height and width. Specifically, the tunneling resistance may be defined as:

$$R_{tunnel} = \frac{h^2 d}{A{q_e}^2\sqrt{2m\lambda}} e^{\frac{4\pi d}{h}\sqrt{2m\lambda}}$$

where h represents Planck's constant, d represents distance between electrodes, q_e is charge of an electron, m is the mass of an electron, and λ represents the tunnel barrier height. Electrons confined in the structure experience a high interfacial barrier if the material has a large effective mass that causes the sub-band to be lowered to near the bottom of the potential well. If there is a mismatch in lattice constants within the material heterostructure, however, an induced strain can modify the bandgap and reduce the barrier height, greatly decreasing the tunneling resistance. For instance, a strain sensor was fabricated with Au nanoparticles (NPs) with tetra(ethylene glycol) dithiol (SH-TEG-SH) linkers to form a covalent 3d network[64]. When the system is strained, the linkers stretch, which increases the AuNP interparticle distance and exponentially increases the tunneling resistance. This allowed them to achieve a gauge factor of 126 in a soft, human-interfaced strain sensor[64]. As these studies have shown, introducing novel mechanisms to increase piezoresistive strain gauge sensitivity can yield gauge factors far above those generated by geometric deformations alone, often exceeding 100 or more, although the higher the gauge factor, typically the lower the linear sensing range. This is because the resistance change in highly sensitive devices is often due to a change in state (like cracking of a microstructure) that occurs at a defined strain, not over a wide range.

B. Piezoelectric Strain Sensors

Strain sensors may also be designed to function based on the piezoelectric effect[65-67]. As shown in Fig 2, the piezoelectric effect occurs when a mechanical deformation creates a dipole moment in a material by deforming the underlying crystal structure, producing a measurable voltage. Because a small deformation can produce a large voltage change in materials with a high d_{33} piezoelectric coefficient, these sensors can be highly sensitive[68]. The gauge factor, and thus sensitivity, of

a piezoelectric strain gauge is defined as the voltage produced per unit force. Because piezoelectric materials are anisotropic, this quantity is related to a material's piezoelectric coefficient depending on the force applied and measurement mode. When the voltage is measured in the same direction of the applied force, as shown in Fig 2, the charge Q is equal to

$$Q = d_{33}F_3$$

where d_{33} is the corresponding piezoelectric coefficient for a 33 direction force-strain relation, and F_3 is the applied force. This is referred to as the longitudinal mode. When the voltage is measured in a direction parallel to the applied force, the charge becomes

$$Q = d_{31}F_1\frac{b}{a}$$

where b and a correspond to the material length in the direction of applied force and measured voltage, respectively. This is referred to as the transverse mode. When measuring a voltage induced by a shear force, the relation becomes

$$Q = d_{51}F_1$$

In each case, the voltage produced at the electrodes is defined as

$$V = \frac{Q}{C}$$

where C is the capacitance of the piezoelectric material and is defined as

$$C = \frac{\varepsilon_0\varepsilon_r A}{t}$$

where ε_0 is the permittivity of free space, ε_r is the permittivity of the material, A is the crystal area, and t is the thickness. We thus see that the gauge factor for a longitudinal mode sensor is

$$GF_{33} = \frac{d_{33}t}{\varepsilon_0\varepsilon_r A}$$

and the gauge factor for a transverse mode sensor is

$$GF_{31} = \frac{d_{31}t\,{}^{b}\!/_{a}}{\varepsilon_0\varepsilon_r A} = \frac{d_{31}b^2}{\varepsilon_0\varepsilon_r a^2 l}$$

where l is the length in the 2 direction, perpendicular to both a and b. Finally, the gauge factor for a shear mode sensor is

$$GF_{51} = \frac{d_{51}t}{\varepsilon_0\varepsilon_r A}$$

In contrast to resistive and capacitive strain sensors, piezoelectric strain sensors produce an instantaneous voltage and do not require continual powering to operate[69]. However, they are often limited by fundamental material properties inherent to the sensing materials that are not desirable for human-interfaced electronics, like low flexibility and stretchability, which in turn limits the sensing range[65, 66]. Judicious patterning in serpentine structures can increase the stretchability by decreasing the localized strain experienced by the sensor, but this in turn decreases the sensitivity[67]. Among the most common materials used for piezoelectric sensors are ZnO NWs, polylactic acid (PLA), and poly(vinylidenefluoride-co-trifluoroethylene) (P(VDF-TrEE))[66-69]. For instance, a wearable strain sensor was developed based on ZnO NWs to detect finger bending[70]. Because the piezoelectric sensor produces an instantaneous voltage based on the deformation, it was furthermore possible to determine the bending speed based on the integral of the voltage signal[70]. Although piezoelectric strain gauges are increasing in prevalence over the last few years, they have not garnered as much attention as other strain sensing mechanisms for human-interfaced electronics because of current limitations in the material flexibility and sensing range[65]. However, the high sensitivity, ranging from 100-500 mV/N makes piezoelectric mode sensors of high interest for future applications should these concerns be resolved.

C. Capacitive Strain Sensors

Geometric changes in a material not only alter its resistance, but they also affect its capacitance. Therefore, it is possible to design simple deformable capacitors to act as strain sensors. The capacitance of a dielectric material may be determined by the following relationship:

$$C = \varepsilon_o\varepsilon_r\frac{lw}{d}$$

where $\varepsilon_o\varepsilon_r$ represent the dielectric constants of a vacuum and the material and l, w, and d are the length, width, and thickness of the dielectric layer, respectively. After experiencing a tensile strain, the capacitor dielectric's length increases to $(1+\varepsilon)l$, whereas the width and thickness decrease to $(1-\nu\varepsilon)w$ and $(1-\nu\varepsilon)d$, respectively. The new capacitance of the material after a tensile strain may thus be expressed as:

$$C_{new} = \varepsilon_o\varepsilon_r\frac{(1+\varepsilon)l(1-\nu\varepsilon)w}{(1-\nu\varepsilon)d} = (1+\varepsilon)C$$

Based on this relationship, it is readily apparent that the theoretical gauge factor, here defined as change in capacitance with strain, for a capacitive strain sensor based on a simple parallel plate capacitor will always be 1 regardless of the Poisson ratio. This is quite low in comparison to state of the art resistive and piezoelectric strain sensors and may not be sufficient for measuring ultra-fine strains from the human body, like those produced by pulses or small gestures[71]. Therefore, numerous works have sought to improve the gauge factor of capacitive strain sensors by utilizing new shapes and judiciously manipulating the mechanical properties of the chosen materials[37, 54, 72-80]. For instance, an interdigitated

electrode structure with AgNW electrodes was embedded in a PDMS substrate to double the gauge factor of their sensor [72, 81]. When the sensor experiences strain perpendicular to the electrode comb, the inter-electrode spacing d increases to $(1+\varepsilon)d$, whereas both the sensors length and thickness decrease to $(1-\nu\varepsilon)l$ and $(1-\nu\varepsilon)w$. Thus the new capacitance in this structure is defined as

$$C_{new} = \varepsilon_o \varepsilon_r \frac{(1-\nu\varepsilon)l(1-\nu\varepsilon)w}{(1+\varepsilon)d}$$

which results in a theoretical gauge factor of -2. In another work, a wrinkled electrode film was employed utilizing a buckling phenomenon to achieve a gauge factor of 3.05 [81]. Recently, auxetic structures that exhibit a negative Poisson ratio have become of increasing interest in the design of highly sensitive strain sensors, and another group used this approach to increase the gauge factor by several times without sacrificing linearity and hysteresis[82]. Another common approach in recent works is to manipulate material properties at the nano-scale to improve the capitors performance. For instance, changes in the interparticle coupling of AuNPs were utilized and their tunnel junctions to create a parallel plate capacitive strain gauge with a gauge factor of 3.5 [83]. Furthermore, Yuan et created a nanocomposite of reduced graphene oxide in a PDMS dielectric, where the anisotropic flakes would align with strain and create microcapacitors that greatly increased in permittivity with strain, allowing for an improved gauge factor of 13.6 [84].

Table 1. Strain sensing approaches

Sensing approach	Mechanism	Gauge factor	Stretchability	Reliability	Linear Operating Range	Hysteresis
Resistive	**Geometric** [24, 42-46]	1-3	10-300%	Very high	10-100%	High
Resistive	**Percolation Threshold** [42, 54, 55]	10-100	10-300%	High	5-30%	High
Resistive	**Crack** [57-60]	100-1000	1-20%	Low	1-10%	Very High
Resistive	**Disconnection** [11, 28, 52, 61, 62]	10-100	1-20%	Medium	1-10%	High
Resistive	**Tunneling** [42, 63-64]	100-1000	10-200%	High	10-100%	Medium
Piezoelectric	**Piezoelectric** [65-69]	100-500 mV/N	1-5%	High	1-5%	Low
Capacitive	**Capacitive** [5, 37, 54, 73-80, 85, 86]	1-10	1-50%	Very high	1-30%	Low

Despite these exciting advances, significant opportunities remain to explore advanced mechanical and material properties at the nano-scale to improve capacitive strain sensors for human-interfaced electronics. Most printed strain sensors implemented in practical on-body applications to date have been based on printed nanomaterial electrodes with either an Ecoflex or PDMS dielectric layer in a parallel plate or interdigitated electrode structure [5, 37, 54, 73-80, 85, 86]. Compared to piezoelectric and resistive strain sensors, capacitive strain sensors are generally highly linear, reliable, simple to fabricate, and low in hysteresis, but they are limited in sensitivity. Typical gauge factors are below 10, even for advanced materials and geometries. As mentioned above, new advances in materials and mechanics for capacitive strain sensors may offer an exciting way to produce highly linear, reliable, and low hysteresis strain sensors that also exhibit exceptional sensitivity.

III. Strain Sensor Fabrication

A. Screen Printing

Screen printing has been used in garment patterning for centuries, and it has become a key fabrication method for a variety of printed electronics because of its high suitability for rapid roll-to-roll manufacturing, ease of prototyping, and simplicity[87, 88]. Screen printing involves the active transfer of ink from a mesh to a target substrate mediated by pressure and sheer applied by a blade termed the squeegee.[89, 90]. Printing occurs in six phases, as shown in Figure 3(A)[89, 91]. First (I), ink enters the mesh in a process termed flooding with the application of gentle pressure[90]. Second (II), the mesh is brought into contact with the substrate as a result of applied pressure from the squeegee as it travels, and the highly pseudoplastic ink thins with applied pressure[92]. Third (III), the ink adheres to the mesh and the substrate in a uniform liquid[91]. Fourth (IV), the mesh is pulled upwards as the squeegee progresses down the print, causing the ink structure to rise and stretch[91]. Fifth (V), the ink forms filament structures between the mesh and substrate as the mesh is further raised[91]. Finally (VI), the filaments collapse and the print levels, resulting in a deposition thickness that depends on the mesh open area and the ink adhesion to both the mesh and the substrate[91, 93]. In traditional screen-printing applications, the substrate is placed on a flat plate below the mesh, as shown in Figure 3(B)[94]. In roll-to-roll screen-printing, the mesh is folded into a cylinder with the squeegee blade positioned inside the cylinder[95]. As the substrate is rolled against the mesh and the impression cylinder, pressure and sheer are applied proportional to the print velocity[95]. This process is depicted in Figure 3(C) [95]. In screen printing, the mesh substrate offset distance and mesh geometry are crucial parameters, but, contrary to popular conception, the squeegee speed and pressure have not been shown to correlate highly with print quality[96]. This is because the sheer and compressive forces in a properly designed ink are sufficient to prevent ink hydroplaning before the squeegee, instead operating solely on the six aforementioned printing stages[97]. Optimizing ink rheology for this complicated fluid dynamics is crucial in screen printing[92]. Ink viscosities are generally high (10-30 PaS), and the inks must be highly pseudoplastic so that they can maintain their structure during flooding, flow easily, and rapidly coalesce without slumping [90, 98].

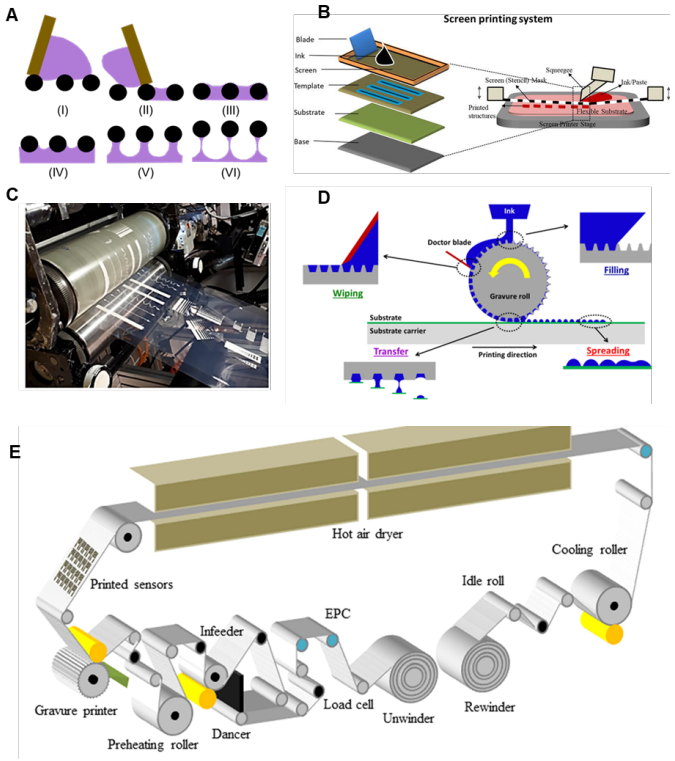

Figure 3. Contact printing methods for nanomaterial-based strain sensors. (A) Illustration of the six stages of screen printing. (reprinted with permission from *ACS Omega* **(2021)**, 6, 14, 9344–9351. Copyright 2021, ACS). Smart Mater. Struct. 27 **(2018)** 085014. (B) Illustration of the screen printing system (Reproduced under a CC-BY 3.0 license from Intech Open DOI: 10.5772/intechopen.89377). (C) Image of a roll-to-roll screen printer used in nanomaterial printing. (reprinted with permission from *Ind. Eng. Chem. Res.* **(2019)**, 58, 43, 19909–19916. (D) Overview of the gravure printing process (reprinted with permission from *Flex. Print. Electron* **2016** 1 023003. (E) Illustration of the complete gravure printing apparatus. (reprinted with permission from Smart Mater. Struct. 27 **(2018)** 085014).

In addition, the area that is not to printed in the mesh is blocked with an emulsion polymer, which must be highly smooth to yield an even print[96]. The minimal resolution achievable in screen printing is limited fundamentally by the mesh quality, even if many inks with suboptimal rheologies cannot approach this limit[90]. Specifically, screen printing meshes are limited by lithography resolution in emulsion etching, emulsion smoothness, and mesh geometries[99]. A finer mesh with more weaves per unit area improves print resolution, but the proportional reduction in mesh open area leads to a thinner print deposition[99]. In summary, screen printing is highly suited for printed strain sensors because it is a mature industrial process with significantly lower startup and prototyping costs than gravure and flexographic printing, and new innovations in mesh or stencil design open new opportunities for increased print resolutions.

B. Gravure Printing

Gravure printing is a mature and widely used manufacturing method that has been employed for high throughput image and newspaper printing since the 19th century[100]. Gravure printing is achieved in four phases, as shown in Figure 3(D), with the overall system schematic shown in Figure 3(E)[94, 100]. First, the ink to be printed is poured on a rotating gravure roll and fills the recessed cells in the roll that comprise the printing pattern[101]. Second, a doctor blade removes excess ink from the gravure roll[101]. Third, the ink is brought in contact with the target substrate, which is itself rolled at the same speed as the gravure roll, and the ink is pulled from the gravure cells onto the substrate as a result of adhesive forces between the ink and the substrate and the ink's intrinsic surface tension[100, 101]. Finally, the print stabilizes on the substrate and spreads into a uniform film from the deposited beads based on the contact angle at the liquid-gas interface on the substrate, which is determined by the Young's equation. $Cos\theta_c = \frac{\gamma_{sg}-\gamma_{sl}}{\gamma_{lg}}$, where $\gamma_{sg}, \gamma_{sl}, \gamma_{lg}$ are the surface energies for solid-liquid, liquid-gas, and solid-gas respectively[30, 100, 102]. In gravure printing, the print resolution, quality, and speed are primarily limited by the complex fluid dynamics occurring when excess ink is removed by the doctor blade, where lubrication residue and ink drag out can occur[100, 103]. First, the doctor blade always leaves a small residual ink layer on the roll because of adhesion between the roll and ink[100].

This residue's thickness depends highly on the capillary number $C_a = \frac{viscous\ forces}{surface\ tension} = \frac{\mu U}{\sigma}$, where μ is the ink viscosity, U is the print speed, and σ is the ink surface tension[102]. At high capillary numbers, the residual thickness is often unacceptable[100]. Therefore, reducing print speed and ink viscosity is essential in limiting lubrication residue. Second, the doctor blade can tend to pull ink out of the cells as it passes and smear the ink on the roll[103]. This process has been analytically and empirically shown to depend primarily on capillary flow, which is limited at high capillary numbers[102, 104]. In practice, achieving a capillary number of Ca≈1 is necessary for high quality gravure printing, although the ideal capillary number also depends on pattern geometry, orientation, substrate wetting, and print thickness[103, 105]. The cell pattern is also crucial in achieving high resolution prints[106]. Printing continuous lines, which is referred to as Intaglio printing, is avoided because the dragout effect is amplified with long prints oriented in the printing direction[107]. To produce high resolution, level prints, minimizing cell dimensions is critical[100, 103, 104]. Traditional print head fabrication methods, like electromechanical and laser engraving, however, cannot produce cells with dimensions <10 μm, and often cause defects in the gravure roll[103, 104]. Therefore, recent works seeking to improve resolutions have employed silicon microfabrication techniques to design very high-resolution gravure rolls[103]. For instance, photolithography was used to design a silicon-based gravure roll capable of producing high resolution traces <30μm with conductivities >10,000 S/m[103].

In summary, gravure printing is a mature process well suited to printing strain gauges, but it also presents very high startup costs, incurs high costs to prototype, places rigid requirements on ink rheology, and often requires substrate surface modifications in order to achieve optimal printing[100, 108, 109].

C. Inkjet Printing

Inkjet printing is among the most ubiquitous graphics printing methods, with exceptionally rapid prototyping and deposition control, making it highly suitable for printed electronics[110-112]. In inkjet printing, pressurized ink is jetted through a nozzle, forming droplets that are deposited onto the substrate and collapse due to impact and the substrate wettability[113]. There are two main methods for inkjet printing, although drop on demand (DOD) printing is greatly preferred over continuous inkjet printing (CIJ) for printed electronics because it yields higher deposition accuracy and resolutions[109]. Illustrations of both methods are provided in Figure 4(A) and (B), respectively [114]. In DOD printing, the ink is jetted through the nozzle by either a piezoelectric actuator or a thermal disturbance that produces a shockwave[110]. A CIJ printer, on the other hand, charges ink droplets and passes them through an electric field, allowing one to control the ink depositions[110]. Both inkjet printing processes are illustrated in Figure 4(a). DOD printing is attractive because it allows for strong control over pattern thickness, high resolution up to 40μm, and inexpensive prototyping, but it is also limited by nozzle clogging, the uneven flow of material to the edge of the print in a process termed the coffee ring effect and reduced throughputs compared to contact printing methods.[115-120].

The fluid mechanics during printing is best characterized by three dimensionless quantities, the Weber number (We), Reynolds number, and Ohnesorge number (Oh):

$$We = \frac{\zeta \rho v^2}{\gamma}$$

$$Re = \frac{\zeta \rho v}{\eta}$$

$$Oh = \frac{\sqrt{We}}{Re} = \frac{\eta}{\sqrt{\zeta \rho \gamma}}$$

where η, ρ, and γ are the ink viscosity, density, and surface tension, respectively, v is the print velocity, and ζ is characteristic printing length, which is in most cases simply the diameter of the print head nozzle[110, 120, 121]. In general, Oh must be between 1 and 1/10 to achieve a quality print, as illustrated in Figure4(b). At high Oh values, the ink viscosity will preclude stable drop formation[119]. When Oh is too low, on the other hand. the ink cannot form a single, well defined drop.[119], and these tradeoffs are illustrated in Figure 4(C) [122]. In addition, the particle size cannot be > ζ/50 in order to avoid nozzle clogging[123]. Another critical challenge in inkjet printing is the coffee ring effect[118].

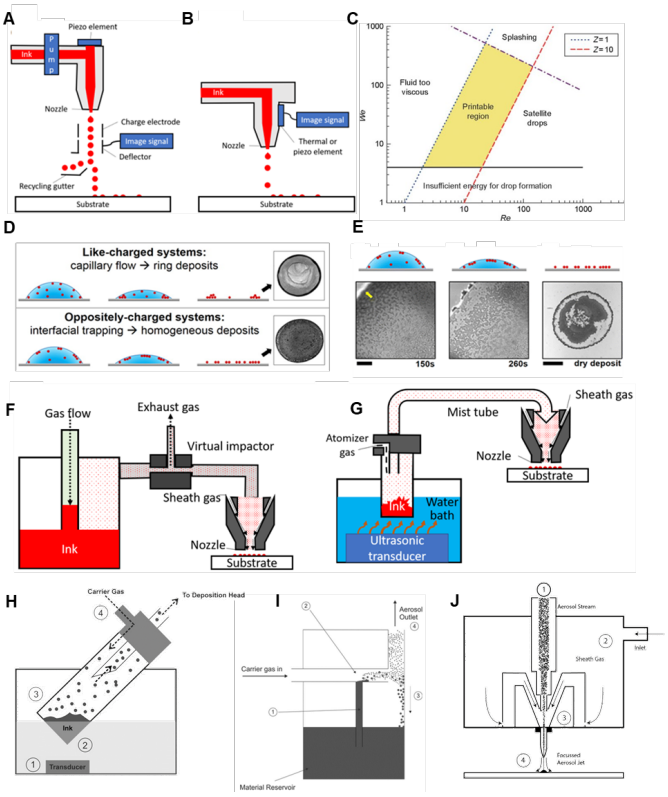

Figure 4. Inkjet and aerosol jet-based strain sensor microfabrication. (A-B) Illustrations of the (A) continuous stream and (B) drop on demand inkjet printing methods (reprinted under a Creative Commons license from J. Manuf. Mater. Process. 2021, 5(3), 89). Optimization space for inkjet printing based on the Weber and Reynolds numbers. (Reprinted under a Creative Commons license from Engineering 1(1), 113-123).) Example images and illustrations of coffee ring formation due to capillary flow in evaporating droplets. (reprinted with permission from *Langmuir* **(2015)**, 31, 14, 4113–4120). (F-G) Schematics of (F) pneumatic and (G) ultrasonic aerosol jet printing (reprinted under a Creative Commons License from J. Manuf. Mater. Process. 2021, 5(3), 89). (H-J) Schematic of (H) ultrasonic and (I) pneumatic atomization and (J) the deposition head. (reprinted under a Creative Commons License from Int. J. Adv. Manuf. Technol. 105, 4599–4619 (2019)).

This occurs when the edge of a droplet on a substrate is fixed in place and capillary flow induced by evaporation of the drop causes material to flow from the interior towards the edge[118]. This process is typically alleviated by Marangoni flow within the drop, but many printing surfactants tend to have very week Marangoni flows[124]. There are many mechanisms under investigation to prevent coffee ring formation, including careful control of the surfactant mediated interactions between particles and the liquid-gas interface[124, 125], mixing high and low boiling point solvents[116], heating the substrate[126], depinning the contact line (which reduces print definition)[127], alternating voltage electrowetting[117], and dual drop inkjet printing[128]. For instance, surfactants were mixed with colloids with opposite charges and observed that

this process produced hydrophobic particles, giving them a greater affinity to the liquid gas interface[125]. These particles on the drop surface prevented capillary flow from collapsing the structure, leading to a uniform deposition, as shown in Figure 4(C-D)[125]. Overall, inkjet printing is highly attractive for printing bioelectronics because complex systems can be very rapidly prototyped during development, then easily scaled to mass production, but there are also very strict requirements on nanomaterial ink properties, lower demonstrated throughputs than alternative methods, and key challenges relating to nozzle clogging that complicate high throughput fabrication.

D. Aerosol Jet Printing

Aerosol jet printing involves the aerosolization of a printable ink in a carrier gas through either pneumatic or ultrasonic atomization[109, 129-136]. The operating principles of pneumatic and ultrasonic aerosol jet printing are illustrated in Fig 6(E) and (F), respectively[136]. As the illustrations show, nanomaterial ink droplets are atomized, then delivered to the ceramic nozzle attached to the print head with a vacuum generated by means of a (typically nitrogen) sheath gas and jetted onto the substrate[136]. The specific atomization mechanisms in ultrasonic and pneumatic atomization are further illustrated in Fig 6(G) and (H), respectively[135, 136]. Finally, the deposition through the nozzle is illustrated in Fig 6(I)[135]. In both mechanisms the jet produced is comprised of many droplets with a diameter of 2–5 μm forced through the nozzle by the carrier gas[135]. In addition to the carrier gas, a sheath gas is used to constrain and constrict the aerosol stream within the nozzle shear. The ratio of the sheath gas flow rate to the carrier gas flow rate is one of the key parameters in aerosol printing, and it must be carefully controlled to prevent overspray and yield high resolution patterns[130]. Similar to inkjet printing, aerosol jet printers are highly susceptible to clogging concerns, placing a critical limitation on ink design[134]. In general, pneumatic atomization is preferred for clogging prevention because it is suited for higher loading percentages (75 vs 50 wt%) and larger particles (50nm vs 500nm), but it is likewise still best by the need for frequent, difficult cleaning that limits throughput[135]. Despite these limitations, aerosol jet printing has been used to demonstrate exceptional spatial control in fine depositions. For instance, one team demonstrated large scale fabrication of complex 3D structures, including spirals and pillars with minimum dimensions of 20 um using aerosol jet deposition of AgNPs dispersed in EG and DI water[137]. Furthermore, well dispersed CNTs, NWs, and graphene may be printed via aerosol jet printing[138-143]. In one example, carboxyl functionalization was used to disperse CNTs with SWCNTs and MWCNTs at a ratio of 80 to 20. They printed the resultant ink using ultrasonic atomization with drop sizes of 1-5 um to yield highly conductive (3 μΩ/cm) traces with widths of only 13 um[138]. Although aerosol jet printing is significantly lower throughput than alternative printing methods and places stringent limitations on ink design, its ability to produce very high-resolution patterns with excellent spatial control, rapid prototyping, and overall deposition quality make it very attractive for printed strain sensor fabrication.

E. Electrohydrodynamic Printing

EHD printing utilizes an electric field to force ink to eject from a conductive nozzle. The overall operating principle of EHD at the nozzle is shown in Fig 5(A)[144]. As the illustration shows, the ink does not eject until some force overcomes the surface tension[136, 144]. Here, this force is produced via electrostatics. Specifically, an electrical potential is applied that causes charge to migrate to the ink meniscus, creating a potential between the meniscus and the grounded substrate. In addition, a tangential electric potential is used to produce a uniform jet, termed the Taylor cone[144]. The electric potential distribution is shown in Fig 5(B) [145]. In order for this method to work, the ink must be suitably dielectric to produce proper charge distributions, or else the resultant jet will be highly non-uniform[146]. Unlike inkjet printing, the Taylor cone in EHD printing can produce a jet smaller than the nozzle head, which greatly assists in producing high resolution patterns when using large nanomaterials that can induce clogging[144]. An illustration of the EHD system is provided in Figure 5(C) [147]. EHD printing is affects strongly by a wide range of printing and ink parameters, which must be optimized in tandem to produce a quality deposition[44, 148-154].

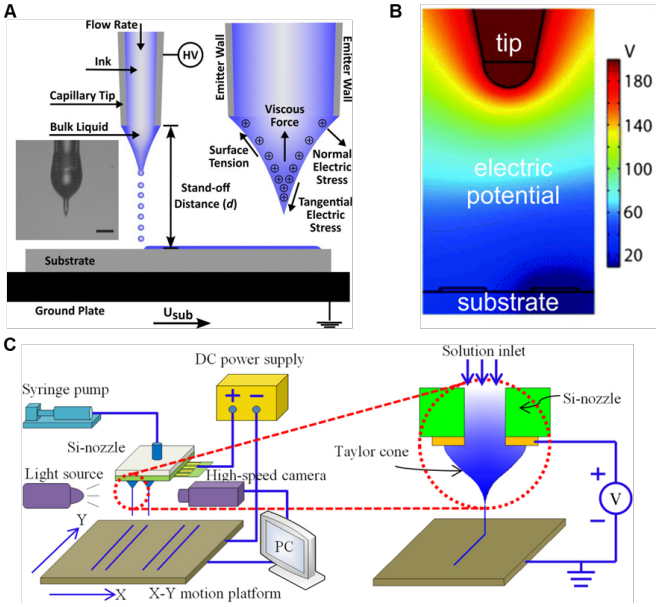

Figure 5. Electrohydrodynamic strain sensor microfabrication. (A) illustration of the physics of EHD printing at the nozzle (reprinted with permission from J. Appl. Phys. 120, 084903 (2016). (B) model showing the spatial distribution of the electric potential during EHD operation around the tip, with the scale bar indicating field strength (reprinted with permission from Nanoscale 2016, 8, 6028). (C) Schematic diagram of the electrohydrodynamic printing system (reprinted with permission from J. Phys. D: Appl. Phys. 46 255301.

For instance, the ink's surface tension, viscosity, and dielectric nature in addition to the printer's substrate offset height, electric potential distribution, nozzle width and length and flow rate are all essential parameters. As a result, stringent requirements are placed on the ink synthesis[44, 148-154]. These inks must have low surface tensions (<50 mN/m) and high viscosities (1-10 Pa S), although increasing both parameters tend to cause print smearing after deposition and reduce resolution[150, 152]. Furthermore, increasing conductivity can increase sensor sensitivity, but it complicates printing by limiting precise surface charge control[148]. Similar to other printing methods, the ink must also be optimized for quality wetting on the substrate, but this is complicated by the need to limit surface tension for EHD printing[149].

In one notable example, a team ball milled a lead zirconate titanate (PZT) powder and prepared a solution of titanium (IV) isopropoxide zirconium (IV) propoxide, lead (II) acetate trihydrate, 1-propanol, and glacial acetic acid with a material loading of 46.7% to yield a printable PZT ink for a piezoelectric strain sensor capable with a d33 of ~66 pC/N[153]. Furthermore, they demonstrated exceptional resolution of 100 um prints with only 5 um inter-line distances. Overall, EHD printing is a very intriguing printing method because the electric field can focus jets to produce very high-quality depositions, but the complicated fabrication method tends to limit printing speed and deposition height while simultaneously complicating ink design. Therefore, additional studies are needed to realize EHD's full potential.

Table 2: Summary of strain sensor fabrication approaches

Method	Printing Speed [m/min]	Typical Min Resolution [μm]	Ink Viscosities [mPa.s]	Surface Tension [mN /m]	Advantages	Limitations
Screen Printing	0.1-15	50	500-10,000	35-50	• Very inexpensive to prototype • Balance between speed, reliability, and cost efficiency • Simple process optimization	• Limited resolution • Strict ink rheology requirements
Gravure	1-20	30	100-500	20-40	• High speed • Good reliability • Long production runs	• High startup costs and expensive prototyping
Inkjet	0.01-15	30	1-20	10-30	• No additional cost to prototype • Excellent resolution and pattern control	• Complicated to integrate with roll-to-roll systems • Nozzle clogging can limit reliability
Aerosol Jet	0.01-1	10	5-10,000	10-50	• Compatible with non-planar surfaces • Rapid prototyping and compatibility with many materials • High resolution	• High susceptibility to clogging • Difficulty in designing printable inks • Low throughput
Electro-hydrodynamic	0.01-0.5	5	100-10,000	20-40	• Excellent resolution • Rapid prototyping	• Low throughput • Difficulty with high deposition heights • High Cost

IV. Materials for Human-Interfaced Strain Sensors

A. Conductive Nanoparticles

NPs are spherical nanomaterials with radii of 10-100 nm that are often formed via wet chemistry methods[155]. In general, NPs tend to agglomerate strongly because of their large surface areas and strong interparticle attractions, which requires the surface to be functionally modified to aid in dispersion[11, 156-158]. Another key limitation of the low aspect ratio is the requirement to have high material loadings to form a conductive network compared to NWs and NTs, which can be a challenge in designing printable inks. However, the low aspect ratio makes sintering at low temperature possible, enabling easy formation into conductive films[64, 156, 159, 160]. The core material can be either a metal, like Au, Ag, Cu, Pt, or Pd, or metal alloy, like Eutectic gallium–indium (EGaIn). Because NPs may be fabricated from many cores and in many geometries and also can be modified in-situ via sintering or other chemical processes, they offer excellent degrees of freedom in design [161]. Indeed, the full potential of NPs for strain gauges has perhaps has not yet been fully explored as a result, and new studies pushing the design boundaries are of great interest. For instance, EGaIn NPs can use a self-healing mechanism based on a passivating oxide skin that protects an internal liquid core to achieve both high sensitivity and reliability [162].

The typical material loadings used for strain gauges are 40–88% dispersed with high concentrations of dispersants, like a 1:1 PVP mixtures[52, 62, 163, 164]. However, the addition of such dispersants alters the ink's printability and lowers the viscosity often below an acceptable level[11, 156-158]. To overcome this challenge, a team mixed a 0.3 M solution of PVP and ethylene glycol (EG) to increase the ability of PVP to bind to the AgNP surface, allowing them to disperse NPs with a 1:2 PVP/$AgNO_3$ ratio[165]. After mixing 60mL of 0.3M PVP-EG solution and 40mL 0.29M $AgNO_3$-EG, the solution was mixed with N, N-dimethylformamide, hydroxyethyl cellulose, and EG to demonstrate a 45 wt% ink with viscosity and rheology suitable for screen printing. After printing on a PI substrate, and sintering at 220ºC, the inks demonstrated a low resistivity of 8.3×10^{-6} Ω·cm, which is only 5 times greater than that of bulk silver[165]. Compared to NWs and NTs, NPs are highly attractive for inkjet printing because of their low aspect ratios, which can avoid nozzle clogging, and they have thus been carefully studied[121]. For instance, Figure 6(A-D) show optical and FFSEM images of an inkjet printed strain gauge along with its performance[140]. In a further example, one group assessed the printability and conductivity of AgNP inks with a variety of solvents and additives, and they determined that a EG, ethanol, ethanolamine, and hyperdispersant (Solsperse 20000) ink with 5.25 mPa.s viscosity resulted in the greatest printability due to the addition of humectants (i.e., ethylene glycol and ethanolamine) combined with low resistivity ($1.6 \times$ 10-4 Ω .cm)[166]. After printing, NP depositions are cured remove any solvents and often sintered to form conductive sheets[167]. Although these sheets are not intrinsically stretchable, they may be utilized for strain gauges based on percolation threshold, cracking, buckling, or disconnection methods [24, 42-46]. Overall, NPs are a simple and low-cost material for strain gauges that can be effectively printed using various methods.

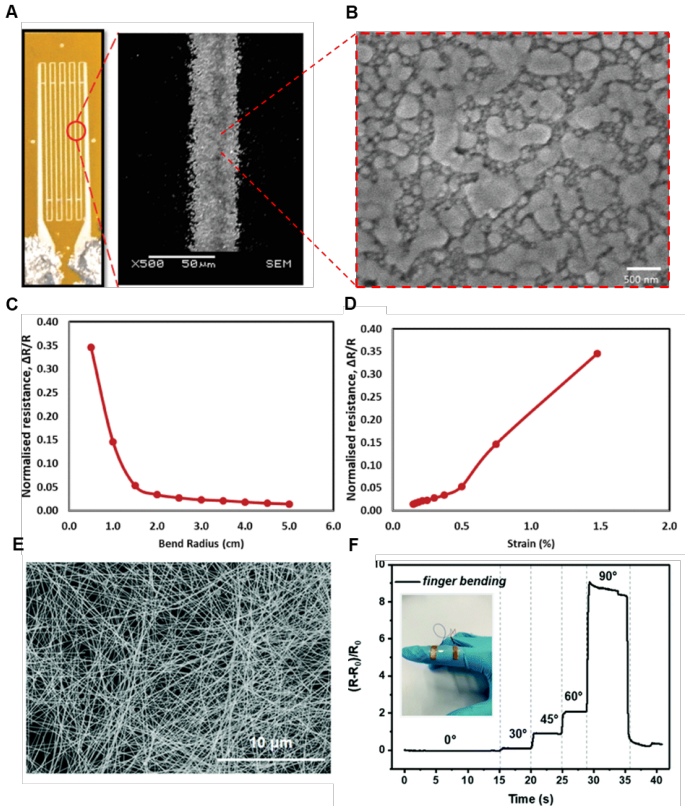

Figure 6. Nanoparticles and nanowires as strain sensing materials (A) Optical image of an aerosol jet printed strain gauge, (B) FESEM image of a silver nanoparticle film after sintering, (C) Change in the normalized resistance with bending radius, and (D) change in normalized resistance strain on the printed sensor. (A-D reprinted under Creative Commons license CC BY 4.0 from *IEEE Access.* **(2018)** 6: 63080-63086.) (E) SEM image of AgNWs printed in a strain gauge. (F) performance of the strain gauge with NWs in (E) during finger bending. (E-F reproduced with permission from Inorg. Chem. Front., **2019**,6, 3119-3124).

Still, they are limited for wearable strain-sensing by low aspect ratios that limit their intrinsic stretchability. This necessitates clever patterning and utilization of advanced strain sensing methods (like the crack mechanism mentioned above) to yield both high sensitivity and effective range.

B. Conductive Nanowires

NWs are high aspect ratio nanomaterials composed of a variety of intrinsic or oxidized metals and semiconducting materials. Typically, their lengths are on the order of 1000 times their widths or greater[168-170]. An image of a NW forest in a printed strain sensor along with the resultant sensor and its performance are shown in Figure 6(E-F)[140]. NW depositions exhibit several highly attractive properties for printed strain gauges based on these aspect ratios[8, 56, 65, 67, 80, 171-181]. When oriented in random directions within a polymer matrix, they easily form conductive networks with low material loadings, greatly simplifying ink design and decreasing bending stiffness, exhibit excellent yield strength near the fundamental limit of E (Young's Modulus) / 10, very high optical transmittance, strong conductivities driven by quantum effects, high stretchability while maintaining conductivity, and potential to tune the strain sensing region based on material loadings[109, 182, 183]. Furthermore, NW inks are significantly easier to synthesize than those comprised of NPs because NWs in random orientations are much more resistant to agglomeration[169]. NW dispersions are also intrinsically stretchable, while sintered NP dispersions are not, but this comes at the cost of lowered conductivity[182]. To overcome this challenge, NWs may be laser welded to form connections only at the wire joints, maintaining stretchability and optical transparency while yielding a highly conductive, sintered connection[169]. For instance, one group used laser welding to demonstrate a highly conductive ($5.0–7.3x10^5$ S/m) AgNW printed film on a flexible PET substrate with similar optical transmittance (>90%) compared to a pure AgNW film[184]. NW inks are primarily fabricated through the polyol method, but the template method is also utilized[30, 169, 170]. In polyol synthesis, the solution temperature, PVP molar ratio to ionic precursor, stirring rate, introduction of platinum seeds or other nucleation agents, and the addition of chloride or bromide ions are key factors to control the NW dimensions and quality[170, 185, 186]. During polyol synthesis, NWs are typically produced from metal seeds reduced from an ionic precursor, like $AgNO_3$, and these seeds are capped by PVP[185, 186]. More studies are needed to create a definitive model for NW growth, but it is theorized that the differential affinity of PVP to the <100> plane than <111> plane in the seed leads to unidirectional growth[187]. Despite a rigorous theoretical model, however, empirical findings allow for precise control of material aspect ratios and purities[186].

Because NWs can achieve conductivity with significantly lower material loadings than NPs (5-15% vs >75%) NW inks can be optimized for high resolution printing. For instance, researchers demonstrated high resolution screen printing of an AgNW ink based on a careful study of material loading and binding and rheological agents[169]. AgNWs with aspect ratios of 500 were mixed with (hydroxypropyl)methyl cellulose (HMC), Zonyl FC-300, and defoamer MO-2170 in a distilled water solution and sonicated[169]. HMC was employed as a viscoelastic polymer with hydroxy groups that bind well to the surface of AgNWs to aid in dispersion and serve as an emulsifier and thickening agent[169]. Zonyl FC-300 decreased the ink's surface tension and promoted substrate wettability, while defoamer MO-2170 was necessary to prevent foaming. It was determined that a 6.6 wt% AgNW ink had the greatest pseudoplasticity and lowest viscoelasticity (i.e. the ink had the highest difference in viscosity during low and high sheer and recovered viscosity the quickest after applied shear was removed), which allowed for screen printing of highly conductive ($4.67x10^4$ S/cm) 50 μm width traces[169]. Researchers conducted a similar study in gravure printed inks

to determine that a 5 wt% ink could yield < 50 µm width traces and 5.34x10^4 S/cm conductivity[30].

One key challenge of NWs is that the high aspect ratios can lead to nozzle clogging in inkjet and aerosol jet printing[182]. To overcome this challenge, one work, for instance, sonicated NWs to reduce particle length, dispersed them in IPA, and optimized inkjet parameters to yield sheet resistances of 8 Ω/□ and conductivities of 10^5 S/m in traces with widths of 1-10mm and thickness of 0.5-2µm after curing at 110 ºC [188]. To reduce clogging, a Dimatix printer with 16 nozzles of diameter 21.5µm spaced 254µm apart was used to create 10pL droplets at 5kHz with a spacing of 20µm and 50% overlap [188]. In summary, NWs are highly attractive for printed strain sensors because of their excellent mechanical stretchability and reliability, high printability and conductivity, and optical transparency, but further work is necessary to unlock their full potential, including careful studies of NW welding and composite structures with NPs, conductive polymers and/or polymer matrices.

C. Carbon Based Materials

CNTs are of great interest for a variety of printed electronics applications, including strain gauges, because of their high elasticity, surface area, aspect ratios, strength, and conductivity, but very strong van der Waals interactions create strong particle agglomeration forces[10, 14, 25, 42, 58, 59, 189-208]. CNTs are comprised of rolled graphene sheets with either one tube (single walled CNT, or SWCNT) or multiple tubes (multi walled CNT, or MWCNT) held together with Van der Waals attractions[209]. An example of grown CNTs is provided in the SEM image in Figure 7(A) [210]. The direction in which CNTs strongly affects the material's properties[211]. "Armchair" CNTs are highly preferred for strain sensors because their identical chiral indices create highly uniform conductivity[212], but zigzag or chiral CNT orientations are widely employed for their semiconducting effects in transistor applications [213]. CNTs are primarily fabricated through three processes: CVD, arc discharge, and laser ablation, although CVD is the most common. In CVD, metal NP seeds of the CNT diameter are used as a catalyst in the presence of a carbon based gas, like CO_2, to form CNTs, and an illustration of this method is provided in Figure 7(B) [213, 214]. To remove the NPs and other impurities, the CNT powder is often sonicated or treated with an acid because CNT purity is key to achieving optimal material properties[35, 189].

As previously mentioned, dispersing CNTs in a printable ink is a key challenge because of their high tendency to agglomerate due to strong interparticle attractions (owing to their highly non-polar surfaces)[212]. This can be overcome by binding an amphiphilic agent to the CNTs that produces a polar region on the CNT surface, allowing the CNTs to be dissolved in a polar ink matrix. For instance, a group dispersed CNTs in an ethanol SDS solution optimized to 7.5 wt%, then added various PVP loadings and assessed printability[35].

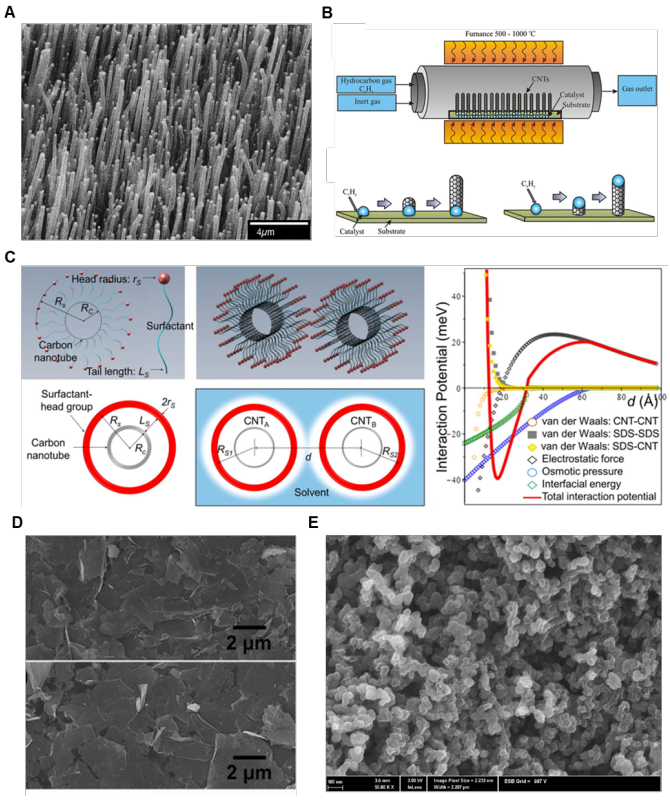

Figure 7. Carbon nanotube, graphene, and bulk carbon-based strain sensors. (A) SEM images of a CNT forest (reprinted with permission from Appl Phys Lett 73(26):3845 – 3847). (B) Schematic representation of the CVD process for CNT synthesis, with illustrations of the base growth (bottom left) and tip growth (bottom right) CNT synthesis methods. (reprinted under a Creative Commons 4.0 License from *Chem. Biol. Technol. Agric.* **(2016)**, 3(17). (C) (A) Mean-density model of surfactant heads for the dispersion of carbon nanotubes (CNTs) with sodium dodecyl sulfate (SDS) with analytically derived potential of mean force for SDS coverage of 70%, reproduced with permission from Appl. Surf. Sci. 2018, 439, 1133-114222). (D) AFM images of screen-printed graphene (reprinted with permission from *J. Colloid Interface Sci.* **(2021)**, 582. (E) SEM images of a carbon black structure (reprinted from permission from Wikimedia Commons).

They found that PVP weights equal to half that of the CNTs were most suited for screen printing[35]. In addition, researchers demonstrated that sonication is crucial in CNT dispersion in the presence of SDS as an amphiphilic agent because the sonication breaks apart CNT clusters, exposing the CNT surface to SDS[215]. An illustration of amphiphilic CNT dispersion is shown is shown in Figure 7(C) [216]. Although developing printable CNT inks is a key challenge, the endeavor is worthwhile because CNTs are among the most highly conductive and durable materials, and their unique properties offer great freedom and new opportunities in strain sensor design, many of which have not been fully explored. In one example, researchers developed a printable CNT ink that showed negative piezoresistivity and low strains and positive piezoresistivity at high strains with very low hysteresis,

enabling them to produce a gauge with high sensitivity in both low and high strain regimes[200]. They hypothesized that these two different operating regions may be attributed to reorientation of CNTs at low strains, followed by separation at high strains[200]. In summary, CNT ink printing is highly attractive for strain gauge fabrication because of their excellent material properties and low cost, and new continued investigations into high throughput fabrication methods are essential in translating these novel discoveries to industrial and clinical use.

The two primary carbon-based materials used in strain gauges are graphene and carbon black. Graphene is a zero-gap semiconductor with exceptional conductivity and high mechanical strength, but it suffers a similar tendency to conglomerate as CNTs due to its highly nonpolar surface[103, 217-219]. An SEM image of printable graphene in shown in Figure 7(D)[36]. Graphene is often formed through exfoliation from graphite, but it may also be synthesized via electrochemical synthesis, chemical vapor deposition, laser processing and sodium ethoxide pyrolysis[217]. To effectively disperse graphene, it can either be oxidized or modified in a manner similar to CNTs. To create a screen printable ink, a team dispersed 5g of graphene nanoplatelets (GNPs) in 50mL EG and 0.5g PVP to aid in dispersion and printed traces on PI with conductivities of 8.81 × 104 S/m[218]. In a gravure printing application, researchers utilized ethyl cellulose (EC) as a dispersion agent to create a highly printable ink[103]. Graphene was exfoliated from graphite in ethanol with EC, and the graphene-EC precipitate was then redispersed in ethanol and terpineol. The loadings of each material were carefully optimized to yield inks with various viscosities, and the optimized ink could be printed with trace widths of <30 µm with conductivities >10,000 S/m[103]. For inkjet printing, researchers exfoliated graphene from graphite in dimethylformamide (DMF), and the toxic DMF was distilled in a terpineol solution[219]. EC was added to protect the graphene from agglomeration. After performing a solvent exchange, the graphene/toluene dispersion was mixed in ethanol in a volume ratio of 3:1 to yield a printable viscosity and rheology. Finally, the resultant ink was printed in 80µm traces on both plastic and silicon substrates to yield supercapacitors with a specific capacitance of 0.59mF cm^{-2}, which is highly attractive for capacitive strain sensing[219].

Carbon black is comprised of over 97% amorphous carbon with a much less carefully arranged structure than that seen in graphene[220]. The carbon is formed into discrete nanoparticles of various sizes and geometries which agglomerate into micro-scale chains and clusters, as seen in the SEM image in Figure 7(E)[221]. These chains and clusters can be highly complex, and their optimization is crucial in controlling dispersion, wettability, conductivity and viscosity when forming printable carbon black inks[221]. Carbon black for printed electronics is typically formed through the furnace black process, although it may be produced as a biproduct of numerous industrial applications[222]. In this process, oil is heated in a furnace, and the temperature, air-to-oil ratio and oil spray position are controlled to partially combust the oil and control the fundamental properties of the carbon black[222]. Because carbon black production is a mature industry requiring expensive equipment, numerous companies have developed printable carbon black inks, but insufficient research into novel carbon black structures, despite the many degrees of freedom in carbon black chain formations, is conducted within academia[78, 222-224]. Regardless, carbon black has been successfully used a strain sensing material in many applications based primarily on commercial inks[19, 57, 78, 223-227]. For instance, one group printed a carbon-black based capacitive strain sensor, where a commercial carbon black ink was printed upon a porous TPU dielectric with sufficient sensitivity to detect micro-strains originating from the human pulse[226].

D. Polymer Based Conductive Materials

Conductive polymer composites (CPCs) are formed by embedding a conductive filler within a stretchable elastomeric polymer. When the polymer undergoes strain, the internal conductive pathways formed by the filler particles are altered due to increased interparticle spacing, resulting in a change in resistance. Typically, an elastomer with a low Young's Modulus, low hysteresis, and excellent mechanical reliability, like poly(dimethylsiloxane) (PDMS), thermoplastic polyurethane (TPU), silicone, or Ecoflex, is selected as the carrier polymer [228]. Then, a conductive filler, like CNTs, carbon black, graphene, NPs, NWs, or a conductive polymer (e.g. PEDOT:PSS, Polyaniline (PANi), or Polypyrrole (PPy)), is introduced to form a conductive network [50, 116, 172, 229]. These fillers are typically introduced either during ink synthesis via mixing in the presence of dispersion agents or during printing by either allowing a printed ink to diffuse throughout an uncured polymer or vice versa or in-situ nanomaterial formation [84, 198, 229]. Material loading during ink synthesis has become the dominant approach in recent works because of the complexity of the diffusion method for mixing during printing; however, both approaches pose significant challenges in material integration [230].

Primarily, all of the aforementioned printing methods have strict rheology requirements and integrate poorly with inks that adhere strongly to the printing apparatus. Therefore, the design of printable inks is of paramount concern, and non-contact printing methods are generally preferred over contact methods because they are less affected by an ink's adhesive properties [229]. For instance, one group created a PEDOT:PSS-MWCNT composite for aerosol jet printing by carefully controlling material fractions to promote aerosol generation, coalescence of the aerosol droplets after deposition, fast drying, and stability [229]. Specifically deionized water, glycerol, and ethylene glycol were mixed in a ratio of 8:1:1 (w/w/w), and the surfactant and adhesion promoter (3-glycidyloxypropyl)trimethoxysilane (GOPS) and the emulsifier carboxymethyl cellulose (CMC) were added to ensure the stability of the structures. The result was an ink printable to 20 µm resolution with a conductivity of 323 S/m. Likewise, a team

formulated a AgNW-Ecoflex composite for inkjet printing and used this approach to fabricate a strain gauge with high sensitivity (a gauge factor of 13.7), a broad strain sensing range over 30%, excellent stability and reliability (>1000 cycles), and low monitoring limit (<5% strain) [231]. In their approach, NWs were formed in-situ by printing potassium halide (KBr:KI:95:5 volume based) and silver nitrate (AgNO3) in the composite ink, which was then exposed to halogen and a D-72 chemical development agent. Further examples of CPCs for strain gauge applications include a carbon black/TPU composite with a GF of 39 [232], a PDMS/CNT composite with a GF of 142 [233], an Ecoflex/PtNP composite with a GF of 42 [234] and an Ecoflex/CNT composite with a GF of 48 [235]. Although significant progress has been made in CPC printing for strain gauges, much remains to be done if their full potential is to be unlocked. The introduction of functional materials offers tremendous degrees of freedom in design, and advanced strain gauge operating principles beyond percolation threshold, crack formation, and wrinkling should be explored (like capacitive and tunneling, for instance). Furthermore, new studies in material integration should be conducted to improve on printable ink design to facilitate high-throughput and high resolution CPC printing beyond what has previously been demonstrated

V. Machine Learning Algorithms

This section aims to cover the current state of machine learning for motion recognition using strain sensors. Motion recognition is an essential component of numerous applications, such as healthcare monitoring, sports performance analysis, and human-computer interaction. The field of machine learning offers a diverse range of techniques that can be effectively applied to motion recognition tasks. For instance, traditional machine learning methods, including support vector machines (SVM), linear discriminant analysis (LDA) and hidden Markov models (HMM), have demonstrated their effectiveness in processing high-dimensional and time-series data. Convolutional neural networks (CNNs), originally developed for computer vision tasks, have been adapted for motion recognition by treating time-series data from strain sensors as input. recurrent neural networks (RNNs) and their advanced counterparts, such as long short-term memory (LSTM) networks and gated recurrent units (GRU), are explicitly designed to handle time-series data and excel at learning long-term dependencies within motion data. In this section, the techniques will be organized into four primary machine learning approaches, each exhibiting unique properties: traditional machine learning, CNN, RNN and Variants, and hybrid models. In order to provide a comprehensive overview, Table 4 presents a comparison of various deep-learning algorithms, focusing on their practical applications and constraints.

A. Traditional Machine Learning

Traditional machine learning, a critical subset of artificial intelligence, includes both supervised and unsupervised learning methods. These techniques have been transformative across various fields, effectively discovering patterns and making informed decisions from data. They hold particular value in the wearable sensing sector, where they have been utilized extensively for tasks such as motion recognition. The models are trained using labeled data in supervised learning, where the desired output is already known. This method is typically used for classification and regression tasks and includes techniques such as Support Vector Machines (SVM), Linear Discriminant Analysis (LDA), and Hidden Markov Models (HMM). On the other hand, unsupervised learning doesn't rely on labeled data. Instead, it uncovers hidden patterns and structures from the input data, making it ideal for clustering and dimensionality reduction tasks. Techniques under this category include Principal Component Analysis (PCA) and t-Distributed Stochastic Neighbor Embedding (t-SNE).

Supervised learning, such as SVM, LDA, and HMM, have been widely used in motion recognition tasks involving strain sensors. SVM is a supervised learning technique used for classification and regression tasks. The main principle behind SVM is to find a decision boundary, called a hyperplane, that best separates different classes in the feature space. The hyperplane is chosen to maximize the margin between the classes, which is the distance between the hyperplane and the nearest data points from each class (called support vectors)[236]. For linearly separable data, the optimal hyperplane can be found by solving an optimization problem that minimizes the norm of the weight vector while ensuring that a margin separates the data points from different classes. For non-linearly separable data, SVMs use kernel functions, such as the Radial Basis Function (RBF) kernel, to map the data into a higher-dimensional space where it can be separated linearly[237]. LDA is another traditional machine learning approach that has been applied in motion recognition tasks with strain sensors. LDA is a supervised learning technique used for dimensionality reduction and classification tasks. It works by projecting the original high-dimensional feature space onto a lower-dimensional space that maximizes the separability between different classes [238]. The projection is achieved by finding a set of linear combinations of the features that best discriminate between the classes[239]. HMM is a probabilistic modeling technique used for time-series data analysis. HMMs consist of a finite set of hidden states and a set of observations associated with each state. Transitions between states and observations follow Markovian properties, which means the probability of the next state or observation depends only on the current state. The model parameters, which include the initial state probabilities, state transition probabilities, and observation probabilities, are learned using the Expectation-Maximization (EM) algorithm or other optimization techniques[240].

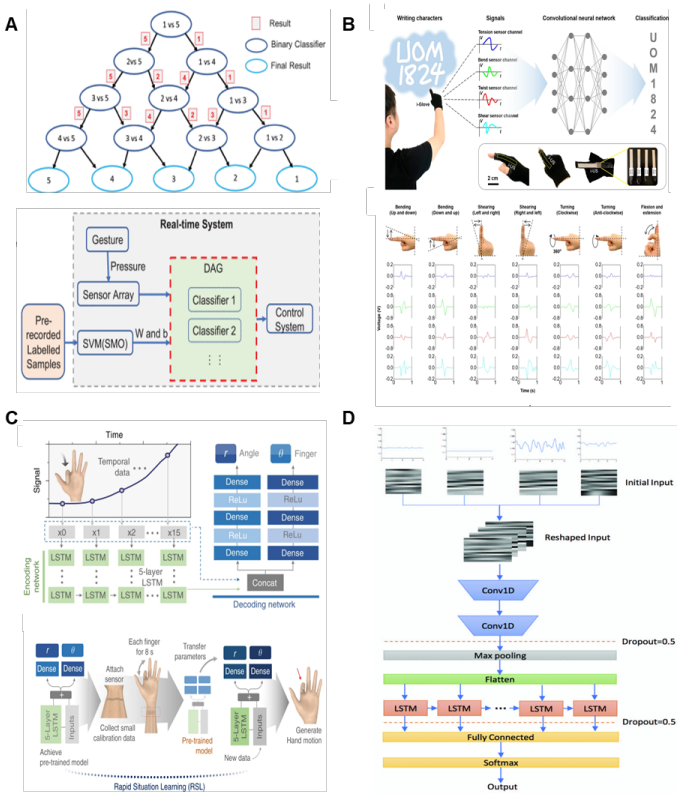

Figure 8. Machine learning approaches for human motion recognition from strain measurements. (A) Schematic Diagram of the real-time system with DAG-SVM classifier for gesture recognition (reprinted under Creative Commons license CC BY 4.0 from *IEEE Access*). (B) CNN with a LeNet-5 based architecture to classify finger movement (for reprinted under Creative Commons license CC BY 4.0 from Spring Nature). (C) Schematic Diagram of the real-time system with LSTM network for Human Computer Interaction (HCI) application (reprinted under Creative Commons license CC BY 4.0 from Spring Nature). (D) Schematic Diagram of the system process with CNN-LSTM hybrid model architecture (reprinted from IEEE Access, copyright ©[2020] IEEE).

SVM, LDA, and HMM have found applications in various motion recognition tasks using strain sensors, such as recognizing different gestures or postures in wearable devices and smart textiles. For instance, one study presented a wrist-worn device equipped with machine learning capabilities and a wearable pressure sensor array for monitoring various hand gestures by tracking tendon movements around the wrist as in Figure 8(A). The array of PDMS-encapsulated capacitive pressure sensors is utilized to capture wrist movement, and the data is processed using a LabVIEW program to visually reconstruct the gestures on a computer. To overcome the uncertainties of tendon movements when the wristband is re-worn or used by a different person, a calibration step based on the SVM learning technique is implemented. The sequential minimal optimization algorithm is also applied to generate SVM classifiers efficiently in real-time. This study demonstrates that the device can accurately classify three distinct gestures with high accuracy (>90%) during real-time gesture recognition[241]. Another study applied SVM to classify various human activities effectively, such as finger and elbow bending and gestures, captured from a strain sensor based on a single-walled carbon nanotube (SWCNTs) and carbon black (CB) synergistic conductive network. After preprocessing the raw sensor data, the SVM algorithm achieved a high accuracy of over 90% in motion recognition tasks, demonstrating its potential in wearable motion recognition applications[225]. Also, the SkinGest system integrates filmy stretchable strain sensors and machine learning algorithms including LDA, KNN, and SVM classifiers, successfully identified American sign language 0-9 with an average accuracy of 98% [13]. Other researchers used stretchable strain gauge sensors to detect hand gestures, and was validated using two machine learning algorithms, LDA and SVM, achieving reproducibility rates of 98% and 94%, respectively[242]. Finally, a study presented a modified barometric pressure sensing approach for wearable hand gesture recognition using LDA, SVM and KNN and finger angle estimation using Random Forest, achieving 90-94% classification accuracy[243]. Furthermore, a master-slave hand operation cooperative perception system using flexible strain sensors and an HMM classifier was developed to achieve a 94.58% accuracy rate in recognizing nine different grasping states with less than two degrees of error in joint angle measurements[244]. Despite their strengths, SVM, LDA, and HMM have limitations. SVMs can be computationally expensive and require careful parameter tuning for optimal performance [245, 246]. LDA has limitations in dealing with non-linear relationships in the data and may not perform well in scenarios where the classes are not clearly separable [247]. On the other hand, HMMs can struggle with complex dependencies in data due to their Markovian property and can also be computationally expensive when dealing with large state spaces or long sequences[248, 249].

Unsupervised machine learning methods, including PCA and t-SNE, have been employed in wearable sensing for motion recognition as well. PCA is an unsupervised learning algorithm used for dimensionality reduction and data visualization. It works by finding orthogonal directions, called principal components, in the original feature space along which the data varies the most[250]. The data can then be projected onto these principal components, reducing its dimensionality while preserving as much of its variation as possible[251]. t-SNE, or t-Distributed Stochastic Neighbor Embedding, is another unsupervised learning algorithm used for data visualization and exploration. It is especially useful for visualizing high-dimensional data in two or three dimensions[252]. t-SNE works by finding a low-dimensional representation of the data that preserves the relative distances between data points as much as possible. It does this by minimizing a cost function that measures the divergence between the distributions of distances in the original and low-dimensional spaces[253]. Researchers have utilized PCA and t-SNE in tasks related to motion recognition. Leveraging PCA,

researchers have developed a high-performance, biomimetic flexible fiber strain sensor inspired by a fish's lateral line scale, capable of accurately monitoring and recognizing micromotions in wearable electronics[254]. Also, the PCA algorithm aided in the management of high-dimensional data from highly sensitive and robust flexible strain sensors, thus improving system performance and achieving over 98% accuracy in sign language recognition[255]. In other research, PCA and a modified t-SNE algorithm were both utilized for fault detection in high-dimensional data, where the latter not only extracted latent data features but also proved superior in preserving local structure and visualizing detection processes, as evidenced by a 100% fault detection rate in specific scenarios[256]. Additionally, t-SNE was effectively applied for dimensionality reduction, where a smart glove equipped with a polyurethane-encapsulated reduced graphene oxide strain sensor precisely recognized ten different gestures, thereby achieving flawless accuracy in a machine learning task using an SVM model[257]. Despite their strengths, unsupervised learning methods also have limitations. PCA assumes that the principal components are orthogonal and therefore may not capture complex dependencies in the data[258]. t-SNE can be sensitive to the choice of tuning parameters and may produce different results for different runs of the algorithm[259]. In conclusion, both supervised and unsupervised learning techniques have their strengths and limitations and have found application in the field of wearable sensing for motion recognition. Future research should continue to explore the utility and applicability of these methods in this rapidly evolving field.

B. Convolutional Neural Networks

Convolutional neural networks (CNNs) are feedforward neural networks designed to process grid-like data, such as images or time-series data. The architecture of a CNN typically comprises several layers, including the input layer, convolutional layers, pooling layers, fully connected layers, and an output layer. Each layer is responsible for transforming the input data into a more abstract representation, ultimately leading to the final output. Convolutional layers are the core building blocks of CNNs. They apply convolution operations to the input data, detecting local patterns and features such as edges, corners, or textures. These layers utilize filters or kernels, which are slid across the input data, generating a feature map. The application of multiple filters in a single convolutional layer allows the network to learn various features simultaneously. Pooling layers reduce the spatial dimensions of the feature maps, aggregating information and reducing computational complexity. The most common pooling operations are max pooling, which selects the maximum value within a defined region, and average pooling, which calculates the average value within the same region. Fully connected layers integrate the extracted features from the previous layers and make predictions based on the learned representations. The final output layer typically employs an activation function, such as a SoftMax function, to produce probabilities for each class or a linear activation function for regression tasks[260].

The unique properties of CNNs that make them suitable for strain sensor data analysis include local connectivity, weight sharing, and hierarchical feature learning. Unlike traditional machine learning algorithms, CNNs have a local receptive field, meaning that each neuron is only connected to a small region of the input data, allowing the network to learn local patterns effectively, which is especially important for spatial or temporal data. CNNs also use the same weights and biases for each filter across the entire input data, significantly reducing the number of trainable parameters and contributing to the network's ability to generalize. This weight sharing property enables the network to detect patterns irrespective of their location within the input data[261]. Furthermore, by stacking multiple convolutional and pooling layers, CNNs can learn complex hierarchical features from the input data. Lower layers capture basic patterns, while deeper layers learn more abstract and high-level features. This hierarchical learning capability enables CNNs to effectively model the complexities of strain sensor data[262].

CNNs have become increasingly popular in recent years due to their exceptional performance in image and signal processing tasks. As a result, they have been successfully applied to strain sensor data analysis, providing more accurate and efficient solutions to various challenges. Figure 8(B) illustrated the use of unimodal strain sensors made of piezoelectric poly L-lactic acid films. These were designed to detect and differentiate individual forces and stresses in human joints, and a CNN with a LeNet-5 based architecture was employed for the classification of finger movements. The resulting system exhibited a mean classification accuracy of 90.2% for seven finger motions and in a finger-air writing application, the classification accuracy was 89.4%. This innovative approach demonstrated the potential for advanced machine learning techniques to improve motion recognition using unimodal strain sensors [263]. In a different study, a deep CNN was applied for golf swing classification. The data originated from smart golf clubs equipped with integrated sensors, including two orthogonally affixed strain gage sensors, a 3-axis accelerometer, and a 3-axis gyroscope. The CNN-based model achieves an accuracy of 95.0[264]. A smart glove was the subject of another study, utilizing ten graphene-coated silk-spandex fabric strain sensors and a LeNet-5 convolutional network for gesture recognition, achieving 96.07% accuracy. The preprocessing included converting sensor signals to joint bending statuses and using real-time visualization with Unity 3D to adapt to a public sign language dataset format[7]. Moreover, other researcher designed a strain sensor using carbonization and polymer-assisted copper deposition combined with a CNN algorithm, which effectively detects and classifies various human body movements, such as normal breathing, tachypnea, and tachypnea with cough, achieving 93.3% real-time accuracy, emphasizing its potential in healthcare applications[265].

Despite their success, CNNs have some limitations. CNNs often face challenges such as requiring large, labeled datasets, and having high computational demands for training, particularly with deep architectures. Additionally, they are prone to overfitting when trained on smaller datasets, leading to poor generalization, and may struggle with task specificity, as their performance may not easily transfer to other tasks or domains. Transfer learning is a powerful technique that helps address some of the limitations of CNNs, such as the need for large datasets, high computational requirements, overfitting, and task specificity. Transfer learning can be applied to CNNs by using the pre-trained weights and architecture from a model trained on a large-scale dataset, such as ImageNet, as a starting point[266]. The CNN's lower layers, which have learned general features like edges, textures, and shapes, are typically kept fixed, while the higher layers are fine-tuned or replaced to adapt the model to the new task. This approach allows for faster training and often better performance compared to training a CNN from scratch, especially when dealing with smaller datasets or related problems.

Transfer learning can be applied to various types of data and problems, including those involving strain sensors. Strain sensors measure the deformation or elongation of materials, and they can produce complex and nonlinear data. If a pre-trained model has already learned features or representations relevant to strain sensor data, it can be fine-tuned for a new task involving strain sensors, potentially leading to faster training and better performance compared to starting from scratch. For instance, one work presented a low-cost, real-time sleeping posture recognition system utilizing a strain sensor array bedsheet and a shallow CNN. By employing transfer learning-based subject-specific methods, the system achieves an accuracy of 91.24%, providing a lightweight and cost-effective solution for monitoring sleep postures while maintaining high performance and privacy[267]. In comparison to other sensor domains, the application of transfer learning for strain sensors has been relatively limited. The primary reason for this is that strain sensor research predominantly revolves around material properties, resulting in considerable variability in the data produced by different types of strain sensors[268]. This leads to a scarcity of pre-trained models or datasets that can be efficiently repurposed for new tasks related to strain sensors. Nevertheless, as the availability of strain sensor data increases and machine learning techniques continue to advance, the potential for transfer learning applications within the strain sensor field is expected to expand in the future.

C. Recurrent Neural Networks and Variants

Recurrent Neural Networks (RNNs) are a class of neural networks that are designed to handle sequential data by maintaining an internal memory state[269]. They are composed of a series of interconnected nodes, where each node receives input from previous nodes in the sequence, as well as from external input data. This allows RNNs to learn and model temporal dependencies in time-series data. Long Short-Term Memory (LSTM) networks are an advanced variant of RNNs to overcome the vanishing gradient problem, which hinders the learning of long-range dependencies in standard RNNs[270]. The LSTM architecture consists of a unique cell state and three gating mechanisms: an input gate, which controls the extent to which new input information is allowed to modify the cell state; a forget gate, which regulates the degree to which the previous cell state is retained; and an output gate, which determines the amount of information from the cell state that is incorporated into the hidden state and passed onto the next node in the sequence. These gates work together to manage the flow of information through the network, allowing LSTMs to effectively capture long-range dependencies within time-series data. Gated Recurrent Units (GRUs) are another RNN variant that offers a simplified architecture compared to LSTM[271]. They have fewer trainable parameters, making them more computationally efficient. GRUs combine the cell state and hidden state into a single hidden state and utilize two gates to control the flow of information: a reset gate, which determines how much of the previous hidden state is retained when computing the candidate hidden state, and an update gate, which balances the contribution of the previous hidden state and the candidate hidden state when computing the new hidden state. A group found that the simplified gating mechanism in GRUs allows them to learn and model temporal dependencies in time-series data with comparable performance to LSTMs but at a lower computational cost[271].

In summary, RNNs and their variants, such as LSTMs and GRUs, have unique architectures designed to capture complex temporal dependencies in time-series data. Their structures enable them to effectively process and analyze sequential data, making them well-suited for strain sensor machine learning research involving time-series data. As depicted in Figure 8(C), one research developed a novel electronic skin integrated with a deep neural network, utilizing a single-channeled sensor and an LSTM network to capture complex hand motions with 96.2% average accuracy. They designed a Rapid Situation Learning (RSL) system that employs transfer learning to adapt the model to new users or different sensor placements in a short time. The system has potential applications in health-monitoring, motion tracking, and soft robotics[6]. Further work has resulted a wearable seamless multimode sensor that accurately recognizes joint motion states with a 97.13% precision using LSTM. This unique sensor decoupled pressure and strain stimuli, offering potential applications in soft robotics, electronic skin, healthcare, and sports systems[12]. In some studies, LSTM network have been utilized to improve the predictability of a soft gold nanowires strain sensor's electrical responses for joint angle measurement applications. The LSTM algorithm enabled the sensor to achieve high accuracy, with an error of less than 2°, for applications such as personal health monitoring and skill assessment[272]. For GRU application, a semi-supervised deep learning method was proposed for calibrating soft microfluidic sensors using only two strain sensors and a GRU-based sequential encoder network. The proposed method was shown

to generate more accurate gait motion with smaller calibration datasets compared to other methods based on supervised deep learning[273].

RNNs, LSTMs, and GRUs, while effective for sequential data, face limitations such as vanishing and exploding gradients, which hinder learning long-range dependencies. They also have high computational complexity and slower processing speeds due to their sequential nature, which can limit performance on modern hardware. Furthermore, these models are task-specific, and their performance may not generalize well across different tasks or domains without additional fine-tuning. Transfer learning which helps address some of the limitations of RNN/LSTM/GRU can be utilized for strain sensor machine learning applications by leveraging pre-trained models from similar tasks to improve performance on a target strain sensor task with limited data. This process typically involves fine-tuning the pre-trained model on the strain sensor dataset, initializing the embedding layer with pre-trained embeddings from related sensor data, and experimenting with different LSTM/RNN architectures. Freezing early layers can help prevent overfitting and optimize transfer learning performance, making it an effective approach for enhancing the efficiency of strain sensor machine learning models. For example, one study explored transfer learning for modeling soft strain sensors in soft robotic applications using LSTM-based recurrent neural networks. This method expedites adaptation to new tasks by minimizing free parameters and training efforts, proving promising for increased sensor dimensionality and data-limited situations[274]. Also, other research presented a wearable sensing brace design and calibration method based on musculoskeletal simulations and LSTM/RNN transfer learning, resulting in improved accuracy, repeatability, and computational efficiency [275].

D. Hybrid Models

CNN-RNN, CNN-LSTM, and CNN-GRU hybrids are all variations of the CNN-RNN hybrid model, combining the strengths of CNNs and RNNs/LSTMs/GRUs to capture both spatial and temporal features in data. In the CNN-RNN hybrid model, the convolutional layers of the CNN extract spatial features from the input data, which are then fed into the RNN to learn and model temporal dependencies. In the CNN-LSTM hybrid model, LSTM cells are used instead of traditional RNN cells, which can better handle long-term dependencies in the input data. Similarly, in the CNN-GRU hybrid model, GRU cells are used instead of RNN cells to improve the model's computational efficiency. The CNN component of the hybrid model can extract important features from the raw sensor data and create meaningful representations of the input data. This is particularly useful in strain sensor data, where the data may contain complex patterns that are difficult to discern through traditional feature extraction methods. The RNN/LSTM/GRU component of the hybrid model can capture the temporal dependencies in the input data and model the sequence of events over time. This is important in strain sensor data, where the strain readings are often taken at regular intervals and the changes over time can be critical for understanding the behavior of the sensor. For instance, researchers proposed a wearable gait motion data acquisition system that uses accelerometers, gyroscopes, and strain gauge sensors to identify gait activities through machine learning. The proposed CNN + RNN hybrid algorithm achieved an accuracy of 98.9%, precision of 96.8%, sensitivity of 97.8%, specificity of 99.1%, and F1-score of 97.3%, showing potential for monitoring gait disorder patients and improving their quality of life[276]. As shown in Figure 8(D), another study developed a highly sensitive, stretchable, and low-cost strain sensor enabled by a conductive thin film for human posture detection with loose-fitting smart garments. They implemented a CNN-LSTM hybrid model to overcome the noise induced by the loose-fitting of the sensors and evaluate the system's feasibility in three case studies. The results show that the proposed E-Jacket smart garment system is capable of recognizing different postures with accuracies ranging from 84.4% to 91.7%, depending on the specific application[277]. Moreover, researchers proposed a deep learning-based calibration and mapping method for full-body motion sensing using a stretchable fabric sensing suit with 20 soft strain sensors. The CNN-LSTM hybrid model named DFM-Net showed a higher accuracy than traditional methods based on mathematical estimation, such as linear regression, with an RMSE of 29.5 mm for overall motions and 38.7 mm for the worst-case motion[41]. A recent study introduced a new, low-cost data glove system based on multiwalled carbon nanotube strain sensors and a hybrid CNN-LSTM model for accurate gesture recognition. The proposed model achieves an average recognition accuracy of 97.5% of 30 gestures with an average recognition time of 2.173 ms based on only five sensors[278]. Lastly, researchers demonstrated an approach using bioinspired multifunctional sensing systems and a modified machine learning algorithm, including a GRU-CNN model, to identify the softness of objects with high accuracy (98.95%) based on piezoelectric signals, and enable adaptive grasping in response to objects with various softness ranges[279].

However, these hybrid models can still be computationally expensive and require a large amount of training data. To address these issues, researchers have explored various techniques, such as model compression and transfer learning. Model compression techniques aim to reduce the number of parameters in the model, leading to reduced computational cost without sacrificing performance. Transfer learning involves using pre-trained models on large datasets and fine-tuning them for specific tasks, allowing for more efficient training and improved accuracy on smaller datasets. However, Transfer learning and model compression are not commonly used in strain sensor research due to the specific trends of this field, as discussed in the CNN and RNN transfer learning sections.

Table 4. Machine learning approaches for strain-based human motion recognition

Algorithm		Property	Advantage	Limitation
Traditional Model	SVM	• supervised learning method that constructs optimal hyperplane in a high-dimensional space to separate data points into different classes	• Effective in high-dimensional spaces • robust to overfitting provides unique and globally optimal solution	• Sensitive to the choice of kernel function • may perform poorly with noisy or overlapping classes • computationally expensive for large datasets
	LDA	• supervised linear transformation method used for dimensionality reduction, which aims to maximize class separability	• Simple and computationally efficient • good for linearly separable classes • reduces dimensionality while preserving class discriminatory information	• Assumes data is normally distributed and the covariances are the same for each class • may perform poorly when assumptions are violates • Sensitive to outliers
	HMM	• model for sequential data, using hidden states that transition over time and generate observable outputs based on probability distributions	• Good for modeling time series or sequence data • captures the dynamic and temporal nature of the data • flexible modeling of stochastic processes	• Assumes the future state depends only on the current state • requires a large amount of training data • computationally expensive for large state spaces
CNN		• Designed for grid-like data, uses convolutional layers for local feature extraction.	• Robust to spatial variations, able to detect local patterns, and efficient parameter sharing	• Limited ability to capture long-range dependencies • not ideal for sequential data • requires large labeled datasets
RNNL and Variants	RNN	• Designed for sequential data, maintains hidden state across time steps	• Captures long-range dependencies • handles variable-length input/output sequences • models temporal dynamics	• Difficulty in learning long-range dependencies • vanishing/exploding gradients • high computational requirements
	LSTM	• A type of RNN with specialized memory cells to store and retrieve information	• Addresses vanishing gradient problem • learns long-range dependencies • preserves information over longer sequences	• Higher computational complexity • more parameters to train • may require large datasets
	GRU	• A type of RNN with gating mechanisms to control information flow	• Addresses vanishing gradient problem • simpler architecture than LSTM • faster training	• Lower capacity to store information compared to LSTM • may not perform as well on complex tasks
CNN-RNN/LSTM Hybrid		• Combines the strengths of CNNs and RNNs/LSTMs, using CNNs for feature extraction and RNNs/LSTMs for sequence modeling	• Captures spatial and temporal dependencies • robust to spatial variations • handles variable-length input/output sequences	• Higher computational complexity • requires large labeled datasets • may suffer from overfitting

VI. Applications

Motion recognition is a rapidly growing field focused on identifying and interpreting human movements, gestures, and postures. This field finds applications in healthcare, sports, rehabilitation, entertainment, and human-computer interaction, among others. A key component in the advancement of this field is the use of strain sensors due to their high sensitivity and versatility. These sensors can detect subtle changes in strain and deformation, which make them suitable for monitoring a wide array of human motions – from full-body movements to minute changes in joint angles and facial expressions. In motion recognition applications, strain sensors play a crucial role in acquiring high-resolution data on muscle activity, joint movements, and other biomechanical parameters. They capture valuable information on the magnitude and direction of human movements, providing a deeper understanding of the dynamic performance of the human body. This wealth of data paves the way for more accurate and personalized motion analysis, training, and rehabilitation programs.

However, the value of the data collected is intrinsically tied to the effectiveness of the processing methods employed; therefore, the selection of machine learning algorithms plays a crucial role. As the complexity of motion recognition tasks increases, so too does the dimensionality of the data, and by extension, the complexity of the processing circuits.[280] In recent years, the emergence of complex, high-dimensional data in tasks like intricate gesture interpretation or multi-joint movement analysis has become commonplace. Processing this data effectively often necessitates the use of advanced machine learning algorithms. This complexity presents a twofold challenge: maintaining high system performance while managing power consumption, particularly in wearable or portable systems[281]. As an example, deep learning techniques, such as convolutional neural networks (CNNs) or recurrent neural networks (RNNs), can handle this high-dimensional data and deliver high recognition accuracy, however they also impose a substantial computational burden. This could potentially lead to increased processing times and elevated power consumption[282].

Recognizing these challenges, there has been a rising trend in developing lighter versions of these complex algorithms that are optimized for low-power and mobile devices. An example is TensorFlow Lite, a production-ready, cross-platform solution for mobile and embedded devices. TensorFlow Lite provides a set of tools to convert and optimize trained TensorFlow models for use on-device, reducing both the computational load and power consumption without significantly compromising accuracy. In the realm of wearable or portable systems, power consumption is of particular importance. These devices often rely on battery power, and maintaining energy efficiency is a critical factor in their practical application. For instance, in a smart glove for sign language interpretation, one might opt to use algorithms like SVM or decision trees, which are less computationally intensive than deep learning models but still provide acceptable recognition performance[283]. Even lighter options such as Linear Discriminant Analysis (LDA) could be considered for tasks that require less complexity[13]. Real-time requirements also play a significant role in algorithm selection. In applications such as sports performance monitoring or physical rehabilitation, immediate feedback is crucial. This need for real-time operation often favors simpler, faster algorithms, even at a slight trade-off in recognition accuracy. Algorithms like k-NN or lightweight versions of RNNs, such as the Long Short-Term Memory networks (LSTM), can offer a good balance between computational complexity, power efficiency, and real-time processing[284].

In conclusion, the development of motion recognition applications with strain sensors demands careful consideration of several key factors: algorithmic complexity, system performance, power consumption, and real-time processing needs. These considerations help guide the design process, resulting in an optimal system that meets the specific requirements of the intended application. The following sections will delve deeper into these complexities as they apply to four primary areas of application: full-body motion recognition, joint angle tracking, hand gesture recognition, and subtle body motion recognition.

A. Full Body Motion Recognition

Full-body motion recognition is the process of identifying and interpreting the movements, gestures, and postures of the entire human body during various activities. This process enables a comprehensive understanding of human motion dynamics, which can be applied to a wide range of applications, such as sports performance assessment, rehabilitation, virtual reality, human-robot interaction, and motion capture for animation or gaming. One study explored the potential of an "all in one" E-textile with dual tactile and tension stimulus response for monitoring athletic movement and form. This approach demonstrated its potential applications in sports like Taekwondo and physical training analysis[285]. In full-body motion recognition, multiple sensors, including strain sensors, are strategically placed on different parts of the body, such as limbs, torso, and joints. These sensors measure the strain experienced during various movements, capturing information on muscle activity, joint movement, and overall body posture. By monitoring the changes in strain over time, researchers can reconstruct and analyze a subject's motion, offering valuable insights into the biomechanics of human movement.

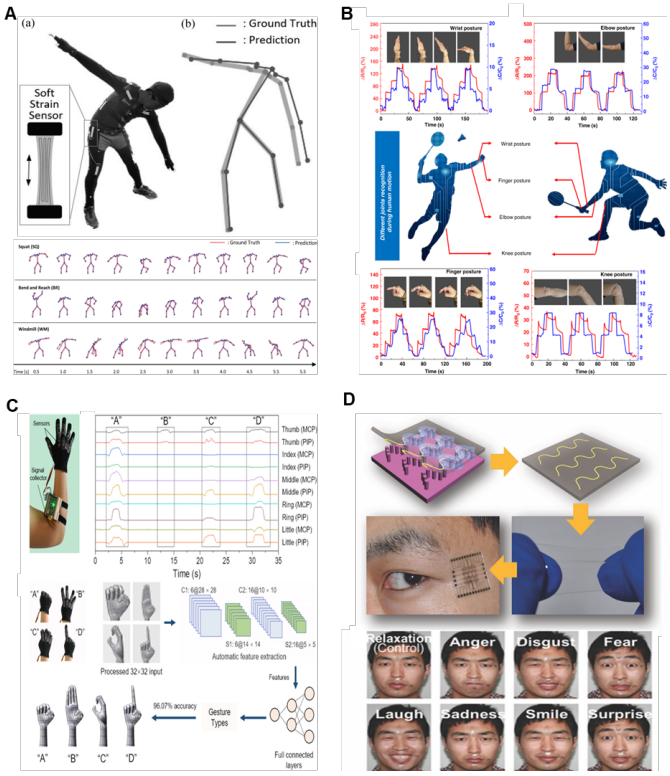

Figure 9. Motion recognition applications in different body parts. (A) Full-body motion recognition using soft strain sensor integrated wearable sensing suit (reprinted from IEEE Access, copyright ©[2019] IEEE). (B) Joint motion recognition using wearable multimode strain-based sensor (reprinted under Creative Commons license CC BY 4.0 from Spring Nature). (C) Hand gesture recognition with graphene strain sensor integrated smart glove (reprinted with permission from Nanotechnology 32 215501 (2021)). (D) Facial expression recognition with multi-analysis flexible strain-based sensor (reprinted with permission from Advanced Materials 28 1369-1374 (2015)).

Further research highlighted the use of a soft sensing shirt with textile-based capacitive strain sensors for tracking shoulder kinematics in 3 DOFs, offering accurate motion tracking for both cyclic and random arm movements[286]. Advancements in sensor technology, such as high sensitivity and flexibility, allow for the unobtrusive integration of strain sensors into clothing or wearable devices. One study demonstrated WCNC (TPU/ACNTs/AgNWs/PDMS) strain sensor with a high conductivity of 3506.8 S/m, a high GF of 1.36 × 105, and a large working strain from 38% to 100%, achieving more precise full-body motion monitoring in multiple directions[287]. This enables continuous monitoring of a wide range of motions, from simple walking and running to complex athletic activities. Another research introduced a wearable soft motion sensing suit for measuring lower extremity joint motion, enabling the study of human biomechanics in various real-life activities.[288] Integration of wireless communication technologies facilitates real-time data transmission and analysis, enabling immediate feedback for athletes or patients to adjust their movements and improve their performance. One instance is a skin-like, recyclable hydrogel sensor designed for comfortable whole-body motion sensing and promoting sustainable wearable electronic device development[289]. Full-body motion recognition using strain sensors also holds potential in virtual reality, gaming, and human-robot interaction, where accurate tracking of the user's body movements can enable more realistic and immersive experiences.

Challenges remain in terms of sensor placement, data processing, and movement classification, necessitating further research to enhance the performance and applicability of strain sensors in full-body motion recognition. For example, researchers presented a soft wearable sensing suit with 20 soft strain sensors for full-body motion tracking as shown in Figure 9(a). By using deep learning-based calibration and mapping methods, the proposed system achieves higher accuracy in motion estimation compared to traditional methods. The experiment results demonstrated that the system is effective in predicting human body poses with an overall root-mean-square-error of 29.5 mm, making it useful for applications in athletics, physical therapy, and virtual reality. However, the need for calibration every time a user wore the sensing suit is a remaining challenge that needs to be addressed in future research. The proposed approach represented a new direction in soft robotics research[41].

B. Joint Angle Tracking

Joint angle tracking refers to the process of measuring and monitoring the angles formed by the relative positions of body segments connected at a joint, such as the elbow, knee, or shoulder. Accurate joint angle tracking is crucial for understanding the biomechanics of human movement, as well as for applications in sports performance assessment,

rehabilitation, physical therapy, and human-computer interaction.

Strain sensors are well-suited for joint angle tracking due to their high sensitivity, flexibility, and ability to detect subtle changes in strain and deformation[290]. To measure joint angles, strain sensors are typically placed near the joint, either on the skin or integrated into wearable devices such as sleeves or braces. As the joint moves, the sensors detect the elongation or contraction of the targeted areas, providing valuable data on the joint's range of motion and angular displacement. This information can then be used to analyze and assess the performance of the joint during various activities, identify abnormalities, or guide the development of personalized training and rehabilitation programs. Notable research included the development of a new stretchable and wearable triboelectric nanogenerator (TENG) sensor to convert mechanical deformation into electrical signals and was used to create a joint sensor and a 3D muscle sensor for real-time human various joint bending monitoring[291]. Another study presented an anisotropic strain sensor to measure unidirectional strain with a root-mean-square error of less than 3° when estimating the angle of a wrist joint[292]. Futhermore, a wearable graphene textile strain sensor has been reported, displaying excellent performance in detecting joint movements and angles, highlighting its potential in wearable electronics and human motion detection applications[293].

Joint angle tracking is essential for evaluating joint health, assessing injury risk, and monitoring the progress of recovery after injury or surgery. Accurate joint angle tracking can also help improve the performance and efficiency of athletes, enabling them to optimize their movements and minimize the risk of injury. As shown in Figure 9(b), this study involved a wearable multimode sensor for joint motion recognition that can decouple pressure and strain stimuli using an independent resistance-capacitance sensing mechanism. The sensor consisted of a resistive and capacitive component and exhibits high strain sensitivity and linear pressure sensitivity. The sensor's dual signal output characteristics allowed for deep learning algorithms to accurately recognize different joint positions and states with 97.13% accuracy. The proposed sensor's low-cost and convenient fabrication process could have potential applications in electronic skin, healthcare, sports monitoring, human-machine interfaces, and soft robot perception systems[12].

In robotics and human-computer interaction, joint angle tracking can facilitate the development of more natural and intuitive interfaces, allowing users to control devices or interact with virtual environments using their body movements. A highlighted study presented an omni-purpose stretchable strain sensor (OPSS) with a nanocracking structure, optimized for monitoring whole-body motions, including joint and skin-level movements. The OPSS sensor has potential applications in medical robotics, wearable healthcare devices, and communication systems for paralyzed patients[294].

C. Hand Gesture Recognition

Hand gesture recognition, from the perspective of strain sensor applications, is a significant advancement in the field of motion recognition. It involves identifying and interpreting specific hand and finger movements for the purpose of communication or interaction with devices and systems. Strain sensors play a crucial role in the development and implementation of hand gesture recognition technology. These sensors facilitate more natural and intuitive interactions, paving the way for seamless communication between users and a wide range of applications[242]. A recent study presented a soft artificial skin with embedded microfluidic strain sensors that can detect hand gestures and finger joint motions, demonstrating promising results in linearity and repeatability[295]. Also, other researchers demonstrated a graphene-based strain sensor with ultra-high gauge factor and a wide strain range, making it suitable hand gesture recognition[296].

Some primary applications of hand gesture recognition that benefit from strain sensor technology include human-computer interaction, virtual reality, gaming, sign language interpretation, and robotics control. For an example of sign language interpretation, this study presented a wearable sign language translation system using a strain sensor which can recognize and display the sign language for all 26 English alphabets by interpreting hand gestures of finger positions in real time[297]. For virtual reality application, researchers demonstrated a wireless, battery-free platform of electronic systems and haptic interfaces capable of softly laminating onto the skin to communicate information via programmable patterns of mechanical vibrations[298]. In each of these contexts, hand gestures provide a seamless way for users to convey information or control systems without the need for conventional input devices like keyboards, mice, or touchscreens. The integration of strain sensors in these applications allows for more accurate and responsive gesture recognition, leading to improved user experiences and increased accessibility for individuals with varying needs and abilities. In another study, researchers introduced a novel electronic skin with an integrated deep neural network which can detect complex hand gestures using a single strain sensor, providing a breakthrough in health-monitoring, motion tracking, and soft robotics applications[6].

As the demand for more immersive and user-friendly interfaces continues to grow, hand gesture recognition supported by advanced strain sensors is expected to play an increasingly important role in the development of modern technology. By leveraging the power of motion recognition systems, hand gesture recognition has the potential to revolutionize how we interact with the digital world and enhance accessibility across a diverse range of applications. As shown in Figure 9(c), this study developed a graphene-coated silk-spandex fabric strain sensor for motion monitoring in wearable devices, demonstrating high sensitivity and durability with a stretch capacity of 60%. Ten sensors were integrated into a smart glove for fine hand movement detection, enabling the

precise tracking of joint angles. The data from the glove was used in a deep learning-based gesture recognition system, utilizing a LeNet-5 convolutional neural network. The gesture recognition system achieved 96.07% accuracy, showcasing the potential of the proposed sensor in human motion detection and machine learning applications[7]. Moreover, other researchers developed a cost-effective, lightweight, wearable sign-to-speech translation system using machine learning, achieving a recognition rate of up to 98.63% and real-time translation in under 1 second. This technology aims to enhance communication between signers and non-signers.[299]. The ongoing advancements in strain sensor technology will continue to drive the progress of hand gesture recognition, ultimately shaping the future of human-computer interaction and beyond.

D. Subtle Body Motion Recognition

Subtle body motion recognition refers to identifying and interpreting small, nuanced, or low-amplitude human movements. These movements can include minor changes in facial expressions, slight hand gestures, or minimal shifts in body posture. Subtle body motion recognition is particularly important in applications requiring a high level of detail and accuracy, such as emotion recognition, sign language interpretation, and human-computer interaction.

Strain sensors can play a crucial role in detecting subtle body motions due to their high sensitivity and ability to measure small changes in strain and deformation. One work showcased a flexible strain sensor with high sensitivity capable of detecting subtle movements with strains as small as 0.1%, which could be used to detect bending, stretching, and facial expression changes[300]. By strategically placing strain sensors on specific body parts, such as the face, hands, or joints, it is possible to capture the minute movements associated with subtle body motions. These sensors can then provide valuable data for further analysis and interpretation, enabling a deeper understanding of the intricate aspects of human movement and behavior. Additionally, other study developed the graphene textile strain sensor which can effectively monitor subtle human motions such as muscle movements, pulse, respiration, and facial expressions, illustrating its potential for various wearable electronics applications[293]. Subtle body motion recognition can be challenging due to the need for high-resolution sensors, accurate data processing, and sophisticated algorithms that can detect and classify the subtle variations in movement. As a result, researchers continue to explore new materials, designs, and techniques to enhance the performance of strain sensors and improve their applicability in subtle body motion recognition. For instance, recent research presented a feasible strategy for the assembly of nanoparticles into controllable micro or nanocurve circuits that could be integrated into a multi-analysis flexible sensor, which could run complicated facial expression recognition. The sensor was made by assembling AgNP curves and could realize arbitrary adjustment of tortuosity morphology, and was capable of tracking eyeball movements, classifying facial expressions, and performing detailed monitoring of the complexed micro muscle group movements as shown in Figure 9(d)[301]. Additional research introduced an ultrathin and durable nanomesh strain gauge designed for continuous facial expression monitoring. This gauges minimized mechanical constraints on natural skin motions and exhibits excellent sustainability, linearity, and durability with low hysteresis[302]. A different study demonstrated patterned graphene strain sensors that can monitor small-scale motions using a simple, scalable, and solution-processable method. These sensors exhibited enhanced sensitivity and can distinguish subtle motions, making them ideal for monitoring subtle human body movements in applications such as acoustic sensing and pulse detection[303].

VII. Conclusions and Future Directions

In recent years, creative and innovative implementations of functional nanomaterials with advanced structures have yielded substantial improvements in human-interfaced strain sensors for motion and gesture recognition. Furthermore, fundamental advances in printing nanomaterials have been developed and leveraged to offer a potential avenue to translate these materials and mechanical innovations into practical applications. However, several key challenges must be overcome if strain sensors are to become ubiquitous tools for human motion recognition, and addressing these opportunities should form the basis for the field's future direction.

First, optimizing strain sensors for the complex challenge of human motion recognition requires considering many variables simultaneously. No prior work has uncovered the optimal material and mechanical innovations necessary to achieve all these requirements. These sensors must be highly stretchable, stable, linear, durable, sensitive, biocompatible, scalable, and possible to integrate with existing electronics. As mentioned throughout the review, novel investigations into traditionally unexplored nanomaterial properties, like auxetic structures, deformable tunneling barriers, and micro-capacitive nanomaterial agglomerations, have shown tremendous promise in addressing some of these fundamental challenges relating to stability, linearity, and sensitivity. Still, they have not been sufficiently studied to meet all these challenges in a fully developed platform. First, more fundamental studies of the material properties are required, and then the sensors may be integrated and studied in functional devices with exceptional performance. Likewise, the devices must be well optimized for the unique challenges afforded by each sensing task, including the ability to decouple multi-directional strains and improve the user experience through both comfort and imperceptibility.

With respect to printing approaches to effectively scale these sensors, recent advances in fundamental printing approaches for gravure, screen, inkjet, aerosol jet, and EHD printing have greatly improved our ability to fabricate complicated and intricate nanomaterial structures, but

significant work remains. In addition, great progress within the last decade on ink rheology optimization for novel printing methods allows for the high-resolution patterning of many functional nanomaterials. This field, however, still has several key challenges to overcome. First, advanced strain sensors increasingly require complex and highly precise patterning and structures, and the further study of printed vias and material adhesion in multiple-layer prints is of high importance. Second, printing resolutions remain low for many methods, and new approaches to increasing resolution must be investigated. Third, inkjet printing offers substantial advantages in prototyping and manufacturing costs. Still, recent works have not implemented commercially tested roll-to-roll inkjet printing to the degree necessary to make inkjet printing a highly attractive method for high throughput nanomaterial fabrication. Printing parameters, like gravure roll geometries and materials, should be thoroughly studied for nanomaterial applications instead of simply relying on processes optimized for inks without high material loadings or dispersion challenges from the traditional printing industry.

Finally, machine learning is a powerful tool that has transformed innumerable industries, but it is only beginning to be well understood for human gesture tracking, which remains a substantial challenge. As sensors become increasingly sensitive and capable of differentiating between strain in multiple axes and improved multi-sensor platforms are developed, new approaches are necessary to improve the number of classes and accuracy possible to achieve with machine learning. Furthermore, algorithm speed and efficiency must be improved to enable real-time classification with high accuracy. From an academic standpoint, developing a set of rules and a framework for determining which algorithm should be implemented and how depending on the application, would greatly assist in developing novel applications. Today, each new application will require a significant investment in time and effort to design new algorithms and implementations, whereas having a structured framework of key insights into algorithm design would greatly assist in the ability to rapidly deploy new optimized strain sensing networks.

Collectively, new studies in materials and mechanics, printing approaches, and machine learning must be conducted in tandem and integrated to yield a fully functional system. Although this achievement may still be many years away, it may be stated with confidence that if the current innovation trend continues, the development of ubiquitous, highly accurate strain-sensing networks is possible. With it, a great benefit to the human condition may be achieved.

VIII. Author Contributions

N.Z. and W.-H.Y. conceived and designed the materials in this paper. All authors conducted reviews of materials and printing technologies, designed figures, and reviewed all sections. All authors wrote the paper together. All authors have read and agreed to the published version of the manuscript.

IX. Funding

We acknowledge the support from the Institute of Information & communications Technology Planning & evaluation (IITP) grant funded by the Korea government (MSIT) (No.2022-0-00025, Development of soft-suit technology to support human motor ability).

X. Conflict of Interest

The authors declare no conflict of interest.

XI. References

[1] S. Zhang, S. Li, Z. Xia, and K. Cai, "A review of electronic skin: soft electronics and sensors for human health," *J Mater Chem B,* vol. 8, no. 5, pp. 852-862, Feb 7 2020, doi: 10.1039/c9tb02531f.

[2] Y. Liu, Y. Hu, J. Zhao, G. Wu, X. Tao, and W. Chen, "Self-Powered Piezoionic Strain Sensor toward the Monitoring of Human Activities," *Small,* vol. 12, no. 36, pp. 5074-5080, Sep 2016, doi: 10.1002/smll.201600553.

[3] X. Liu, Y. Wei, and Y. Qiu, "Advanced Flexible Skin-Like Pressure and Strain Sensors for Human Health Monitoring," *Micromachines (Basel),* vol. 12, no. 6, Jun 14 2021, doi: 10.3390/mi12060695.

[4] G. Ge, W. Huang, J. Shao, and X. Dong, "Recent progress of flexible and wearable strain sensors for human-motion monitoring," *Journal of Semiconductors,* vol. 39, no. 1, 2018, doi: 10.1088/1674-4926/39/1/011012.

[5] S. Yao, L. Vargas, X. Hu, and Y. Zhu, "A novel finger kinematic tracking method based on skin-like wearable strain sensors," *IEEE Sensors Journal,* vol. 18, no. 7, pp. 3010-3015, 2018.

[6] K. K. Kim *et al.*, "A deep-learned skin sensor decoding the epicentral human motions," *Nature communications,* vol. 11, no. 1, p. 2149, 2020.

[7] X. Song *et al.*, "A graphene-coated silk-spandex fabric strain sensor for human movement monitoring and recognition," *Nanotechnology,* vol. 32, no. 21, p. 215501, 2021.

[8] N. Tang *et al.*, "A Highly Aligned Nanowire ‐ Based Strain Sensor for Ultrasensitive Monitoring of Subtle Human Motion," *Small,* vol. 16, no. 24, p. 2001363, 2020.

[9] B. Sindhu, A. Kothuru, P. Sahatiya, S. Goel, and S. Nandi, "Laser-induced graphene printed wearable flexible antenna-based strain sensor for wireless human motion monitoring," *IEEE Transactions on Electron Devices,* vol. 68, no. 7, pp. 3189-3194, 2021.

[10] N. Qaiser, F. Al ‐ Modaf, S. M. Khan, S. F. Shaikh, N. El ‐ Atab, and M. M. Hussain, "A Robust Wearable Point ‐ of ‐ Care CNT ‐ Based Strain Sensor for Wirelessly Monitoring Throat ‐ Related Illnesses,"

Advanced Functional Materials, vol. 31, no. 29, p. 2103375, 2021.

[11] J. Lee *et al.*, "A stretchable strain sensor based on a metal nanoparticle thin film for human motion detection," *Nanoscale,* vol. 6, no. 20, pp. 11932-11939, 2014.

[12] L. Wen *et al.*, "Wearable multimode sensor with a seamless integrated structure for recognition of different joint motion states with the assistance of a deep learning algorithm," *Microsystems & Nanoengineering,* vol. 8, no. 1, p. 24, 2022.

[13] L. Li, S. Jiang, P. B. Shull, and G. Gu, "SkinGest: artificial skin for gesture recognition via filmy stretchable strain sensors," *Advanced Robotics,* vol. 32, no. 21, pp. 1112-1121, 2018.

[14] Z. Sun *et al.*, "Skin-like ultrasensitive strain sensor for full-range detection of human health monitoring," *ACS applied materials & interfaces,* vol. 12, no. 11, pp. 13287-13295, 2020.

[15] Y. Khan, A. Thielens, S. Muin, J. Ting, C. Baumbauer, and A. C. Arias, "A New Frontier of Printed Electronics: Flexible Hybrid Electronics," *Adv Mater,* vol. 32, no. 15, p. e1905279, Apr 2020, doi: 10.1002/adma.201905279.

[16] K. A and L. A, "Mechanical Behaviour of Skin: A Review," *Journal of Material Science & Engineering,* vol. 5, no. 4, 2016, doi: 10.4172/2169-0022.1000254.

[17] N. Zavanelli, S. H. Lee, M. Guess, and W. H. Yeo, "Soft wireless sternal patch to detect systemic vasoconstriction using photoplethysmography," *iScience,* vol. 26, no. 3, p. 106184, Mar 17 2023, doi: 10.1016/j.isci.2023.106184.

[18] N. Zavanelli *et al.*, "At-home wireless monitoring of acute hemodynamic disturbances to detect sleep apnea and sleep stages via a soft sternal patch," *Sci Adv,* vol. 7, p. eabl4146 2021.

[19] R. Goldoni *et al.*, "Stretchable nanocomposite sensors, nanomembrane interconnectors, and wireless electronics toward feedback–loop control of a soft earthworm robot," *ACS Applied Materials & Interfaces,* vol. 12, no. 39, pp. 43388-43397, 2020.

[20] M. Amjadi, K. U. Kyung, I. Park, and M. Sitti, "Stretchable, skin‐mountable, and wearable strain sensors and their potential applications: a review," *Advanced Functional Materials,* vol. 26, no. 11, pp. 1678-1698, 2016.

[21] M. Guess, N. Zavanelli, and W. H. Yeo, "Recent Advances in Materials and Flexible Sensors for Arrhythmia Detection," *Materials (Basel),* vol. 15, no. 3, Jan 18 2022, doi: 10.3390/ma15030724.

[22] R. Sliz *et al.*, "Reliability of R2R-printed, flexible electrodes for e-clothing applications," *npj Flexible Electronics,* vol. 4, no. 1, 2020, doi: 10.1038/s41528-020-0076-y.

[23] Y. Si, S. Chen, M. Li, S. Li, Y. Pei, and X. Guo, "Flexible strain sensors for wearable hand gesture recognition: from devices to systems," *Advanced Intelligent Systems,* vol. 4, no. 2, p. 2100046, 2022.

[24] N. Lu, C. Lu, S. Yang, and J. Rogers, "Highly sensitive skin‐mountable strain gauges based entirely on elastomers," *Advanced Functional Materials,* vol. 22, no. 19, pp. 4044-4050, 2012.

[25] S. J. Park, J. Kim, M. Chu, and M. Khine, "Highly flexible wrinkled carbon nanotube thin film strain sensor to monitor human movement," *Advanced Materials Technologies,* vol. 1, no. 5, p. 1600053, 2016.

[26] S.-Y. Jeong, Y.-W. Ma, J.-U. Lee, G.-J. Je, and B.-s. Shin, "Flexible and highly sensitive strain sensor based on laser-induced graphene pattern fabricated by 355 nm pulsed laser," *Sensors,* vol. 19, no. 22, p. 4867, 2019.

[27] R. Kitsomboonloha, S. Morris, X. Rong, and V. Subramanian, "Femtoliter-scale patterning by high-speed, highly scaled inverse gravure printing," *Langmuir,* vol. 28, no. 48, pp. 16711-16723, 2012.

[28] J. Park, D. Nam, S. Park, and D. Lee, "Fabrication of flexible strain sensors via roll-to-roll gravure printing of silver ink," *Smart Materials and Structures,* vol. 27, no. 8, p. 085014, 2018.

[29] R. A. T. Abbel, Pit ; Rubingh, Eric; van Lammeren, Tim; Cauchois, Romain; Everaars, Marcel; Valeton, Joost; van de Geijn, Sjeord; Groen, Pim, "Industrial-scale inkjet printed electronics
manufacturing—production up-scaling from
concept tools to a roll-to-roll pilot line," *Transl. Mater. Res.,* vol. 1, 015002, 2014, doi: 10.1088/2053-1613/1/1/015002.

[30] Q. Huang and Y. Zhu, "Gravure Printing of Water-based Silver Nanowire ink on Plastic Substrate for Flexible Electronics," *Sci Rep,* vol. 8, no. 1, p. 15167, Oct 11 2018, doi: 10.1038/s41598-018-33494-9.

[31] J. Izdebska, "Chapter 11: Flexographic Printing," *Printing on Polymers*
Fundamentals and Applications, pp. 179-197, 2016.

[32] D. S. Kinnamon, S. Krishnan, S. Brosler, E. Sun, and S. Prasad, "Screen Printed Graphene Oxide Textile Biosensor for Applications in Inexpensive and Wearable Point-of-Exposure Detection of Influenza for At-Risk Populations," *Journal of The Electrochemical Society,* vol. 165, no. 8, pp. B3084-B3090, 2018, doi: 10.1149/2.0131808jes.

[33] N. Zavanelli, J. Kim, and W. H. Yeo, "Recent Advances in High-Throughput Nanomaterial Manufacturing for Hybrid Flexible Bioelectronics," *Materials (Basel),* vol. 14, no. 11, May 31 2021, doi: 10.3390/ma14112973.

[34] N. Zavanelli and W. H. Yeo, "Advances in Screen Printing of Conductive Nanomaterials for Stretchable

Electronics," *ACS Omega,* vol. 6, no. 14, pp. 9344-9351, Apr 13 2021, doi: 10.1021/acsomega.1c00638.

[35] H. Menon, R. Aiswarya, and K. P. Surendran, "Screen printable MWCNT inks for printed electronics," *RSC Advances,* vol. 7, no. 70, pp. 44076-44081, 2017, doi: 10.1039/c7ra06260e.

[36] E. B. Secor, S. Lim, H. Zhang, C. D. Frisbie, L. F. Francis, and M. C. Hersam, "Gravure printing of graphene for large‐area flexible electronics," *Advanced materials,* vol. 26, no. 26, pp. 4533-4538, 2014.

[37] K. Li, H. Wei, W. Liu, H. Meng, P. Zhang, and C. Yan, "3D printed stretchable capacitive sensors for highly sensitive tactile and electrochemical sensing," *Nanotechnology,* vol. 29, no. 18, p. 185501, 2018.

[38] J. Pena-Bahamonde, H. N. Nguyen, S. K. Fanourakis, and D. F. Rodrigues, "Recent advances in graphene-based biosensor technology with applications in life sciences," *J Nanobiotechnology,* vol. 16, no. 1, p. 75, Sep 22 2018, doi: 10.1186/s12951-018-0400-z.

[39] Z. Wan, N.-T. Nguyen, Y. Gao, and Q. Li, "Laser induced graphene for biosensors," *Sustainable Materials and Technologies,* vol. 25, 2020, doi: 10.1016/j.susmat.2020.e00205.

[40] Z. Wan *et al.*, "Laser-Reduced Graphene: Synthesis, Properties, and Applications," *Advanced Materials Technologies,* vol. 3, no. 4, 2018, doi: 10.1002/admt.201700315.

[41] D. Kim, J. Kwon, S. Han, Y.-L. Park, and S. Jo, "Deep full-body motion network for a soft wearable motion sensing suit," *IEEE/ASME Transactions on Mechatronics,* vol. 24, no. 1, pp. 56-66, 2018.

[42] N. Hu, H. Fukunaga, S. Atobe, Y. Liu, and J. Li, "Piezoresistive strain sensors made from carbon nanotubes based polymer nanocomposites," *Sensors,* vol. 11, no. 11, pp. 10691-10723, 2011.

[43] K. Kanao *et al.*, "Highly selective flexible tactile strain and temperature sensors against substrate bending for an artificial skin," *Rsc Advances,* vol. 5, no. 38, pp. 30170-30174, 2015.

[44] S. Khan, S. Ali, A. Khan, M. Ahmed, B. Wang, and A. Bermak, "Inkjet printing of multi-stripes based deflection monitoring sensor on flexible substrate," *Sensors and Actuators A: Physical,* vol. 323, p. 112638, 2021.

[45] M. Li, S. Chen, B. Fan, B. Wu, and X. Guo, "Printed flexible strain sensor array for bendable interactive surface," *Advanced Functional Materials,* vol. 30, no. 34, p. 2003214, 2020.

[46] X. Liao, W. Song, X. Zhang, H. Huang, Y. Wang, and Y. Zheng, "Directly printed wearable electronic sensing textiles towards human–machine interfaces," *Journal of Materials Chemistry C,* vol. 6, no. 47, pp. 12841-12848, 2018.

[47] F. Michelis, L. Bodelot, Y. Bonnassieux, and B. Lebental, "Highly reproducible, hysteresis-free, flexible strain sensors by inkjet printing of carbon nanotubes," *Carbon,* vol. 95, pp. 1020-1026, 2015.

[48] A. Nakamura, T. Hamanishi, S. Kawakami, and M. Takeda, "A piezo-resistive graphene strain sensor with a hollow cylindrical geometry," *Materials Science and Engineering: B,* vol. 219, pp. 20-27, 2017.

[49] X. Wang, J. Sparkman, and J. Gou, "Strain sensing of printed carbon nanotube sensors on polyurethane substrate with spray deposition modeling," *Composites Communications,* vol. 3, pp. 1-6, 2017.

[50] Y. Wang *et al.*, "Flexible electrically resistive-type strain sensors based on reduced graphene oxide-decorated electrospun polymer fibrous mats for human motion monitoring," *Carbon,* vol. 126, pp. 360-371, 2018.

[51] Y.-F. Wang *et al.*, "Printed strain sensor with high sensitivity and wide working range using a novel brittle–stretchable conductive network," *ACS applied materials & interfaces,* vol. 12, no. 31, pp. 35282-35290, 2020.

[52] S. Yoon and H.-K. Kim, "Cost-effective stretchable Ag nanoparticles electrodes fabrication by screen printing for wearable strain sensors," *Surface and Coatings Technology,* vol. 384, p. 125308, 2020.

[53] Č. Žlebič *et al.*, "Comparison of resistive and capacitive strain gauge sensors printed on polyimide substrate using ink-jet printing technology," in *2014 29th International Conference on Microelectronics Proceedings-MIEL 2014*, 2014: IEEE, pp. 141-144.

[54] S. Harada, K. Kanao, Y. Yamamoto, T. Arie, S. Akita, and K. Takei, "Fully printed flexible fingerprint-like three-axis tactile and slip force and temperature sensors for artificial skin," *ACS nano,* vol. 8, no. 12, pp. 12851-12857, 2014.

[55] R. Herbert, H.-R. Lim, and W.-H. Yeo, "Printed, soft, nanostructured strain sensors for monitoring of structural health and human physiology," *ACS applied materials & interfaces,* vol. 12, no. 22, pp. 25020-25030, 2020.

[56] M. Amjadi, A. Pichitpajongkit, S. Lee, S. Ryu, and I. Park, "Highly stretchable and sensitive strain sensor based on silver nanowire–elastomer nanocomposite," *ACS nano,* vol. 8, no. 5, pp. 5154-5163, 2014.

[57] S. Jang *et al.*, "Carbon-based, ultraelastic, hierarchically coated fiber strain sensors with crack-controllable beads," *ACS applied materials & interfaces,* vol. 11, no. 16, pp. 15079-15087, 2019.

[58] H. Sun *et al.*, "A highly sensitive and stretchable yarn strain sensor for human motion tracking utilizing a wrinkle-assisted crack structure," *ACS applied materials & interfaces,* vol. 11, no. 39, pp. 36052-36062, 2019.

[59] Y. Zhou *et al.*, "Significant stretchability enhancement of a crack-based strain sensor combined with high sensitivity and superior durability for motion monitoring," *ACS applied materials & interfaces,* vol. 11, no. 7, pp. 7405-7414, 2019.

[60] J. Tolvanen, J. Hannu, and H. Jantunen, "Stretchable and washable strain sensor based on cracking structure for human motion monitoring," *Scientific Reports,* vol. 8, no. 1, p. 13241, 2018.

[61] X. Guo *et al.*, "Ultra-sensitive flexible piezoresistive pressure sensor prepared by laser-assisted copper template for health monitoring," *Sensors and Actuators A: Physical,* vol. 334, p. 113325, 2022.

[62] W. Zhang, Q. Liu, and P. Chen, "Flexible strain sensor based on carbon black/silver nanoparticles composite for human motion detection," *Materials,* vol. 11, no. 10, p. 1836, 2018.

[63] J. Song *et al.*, "Hierarchical Reduced Graphene Oxide Ridges for Stretchable, Wearable, and Washable Strain Sensors," *ACS Appl Mater Interfaces,* vol. 11, no. 1, pp. 1283-1293, Jan 9 2019, doi: 10.1021/acsami.8b18143.

[64] C. B. Huang *et al.*, "Highly Sensitive Strain Sensors Based on Molecules‐Gold Nanoparticles Networks for High‐Resolution Human Pulse Analysis," *Small,* vol. 17, no. 8, p. 2007593, 2021.

[65] Z. Huo *et al.*, "High-performance Sb-doped p-ZnO NW films for self-powered piezoelectric strain sensors," *Nano Energy,* vol. 73, p. 104744, 2020.

[66] M. Kozioł, B. Toroń, P. Szperlich, and M. Jesionek, "Fabrication of a piezoelectric strain sensor based on SbSI nanowires as a structural element of a FRP laminate," *Composites Part B: Engineering,* vol. 157, pp. 58-65, 2019.

[67] M. Panth *et al.*, "High-performance strain sensors based on vertically aligned piezoelectric zinc oxide nanowire array/graphene nanohybrids," *ACS Applied Nano Materials,* vol. 3, no. 7, pp. 6711-6718, 2020.

[68] M. Zhu, N. Inomata, N. Adachi, A. Sakurai, M. Nomura, and T. Ono, "High-gauge factor strain sensor based on piezoelectric aluminum nitride coupled to MOSFET," *IEEE Sensors Journal,* vol. 19, no. 10, pp. 3626-3632, 2019.

[69] Y. Tian, P. He, B. Yang, Z. Yi, L. Lu, and J. Liu, "A flexible piezoelectric strain sensor array with laser-patterned serpentine interconnects," *IEEE Sensors Journal,* vol. 20, no. 15, pp. 8463-8468, 2020.

[70] S. Y. Chung, H.-J. Lee, T. I. Lee, and Y. S. Kim, "A wearable piezoelectric bending motion sensor for simultaneous detection of bending curvature and speed," *RSC Advances,* vol. 7, no. 5, pp. 2520-2526, 2017, doi: 10.1039/c6ra25797f.

[71] J. Wang, C. Lu, and K. Zhang, "Textile‐based strain sensor for human motion detection," *Energy & Environmental Materials,* vol. 3, no. 1, pp. 80-100, 2020.

[72] S. R. Kim, J. H. Kim, and J. W. Park, "Wearable and Transparent Capacitive Strain Sensor with High Sensitivity Based on Patterned Ag Nanowire Networks," *ACS Appl Mater Interfaces,* vol. 9, no. 31, pp. 26407-26416, Aug 9 2017, doi: 10.1021/acsami.7b06474.

[73] E. R. Cholleti, J. Stringer, M. Assadian, V. Battmann, C. Bowen, and K. Aw, "Highly stretchable capacitive sensor with printed carbon black electrodes on barium titanate elastomer composite," *Sensors,* vol. 19, no. 1, p. 42, 2018.

[74] A. Frutiger *et al.*, "Capacitive soft strain sensors via multicore–shell fiber printing," *Advanced Materials,* vol. 27, no. 15, pp. 2440-2446, 2015.

[75] K. T. Fujimoto *et al.*, "Aerosol jet printed capacitive strain gauge for soft structural materials," *npj Flexible Electronics,* vol. 4, no. 1, p. 32, 2020.

[76] A. V. Quintero *et al.*, "Capacitive strain sensors inkjet-printed on pet fibers for integration in industrial textile," *Procedia engineering,* vol. 120, pp. 279-282, 2015.

[77] J. Shintake, Y. Piskarev, S. H. Jeong, and D. Floreano, "Ultrastretchable strain sensors using carbon black‐filled elastomer composites and comparison of capacitive versus resistive sensors," *Advanced Materials Technologies,* vol. 3, no. 3, p. 1700284, 2018.

[78] V. Tsouti, V. Mitrakos, P. Broutas, and S. Chatzandroulis, "Modeling and development of a flexible carbon black-based capacitive strain sensor," *IEEE Sensors Journal,* vol. 16, no. 9, pp. 3059-3067, 2016.

[79] S.-J. Woo, J.-H. Kong, D.-G. Kim, and J.-M. Kim, "A thin all-elastomeric capacitive pressure sensor array based on micro-contact printed elastic conductors," *Journal of Materials Chemistry C,* vol. 2, no. 22, pp. 4415-4422, 2014.

[80] S. Yao and Y. Zhu, "Wearable multifunctional sensors using printed stretchable conductors made of silver nanowires," *Nanoscale,* vol. 6, no. 4, pp. 2345-2352, 2014.

[81] R. Nur, N. Matsuhisa, Z. Jiang, M. O. G. Nayeem, T. Yokota, and T. Someya, "A Highly Sensitive Capacitive-type Strain Sensor Using Wrinkled Ultrathin Gold Films," *Nano Lett,* vol. 18, no. 9, pp. 5610-5617, Sep 12 2018, doi: 10.1021/acs.nanolett.8b02088.

[82] J. Shintake, T. Nagai, and K. Ogishima, "Sensitivity Improvement of Highly Stretchable Capacitive Strain Sensors by Hierarchical Auxetic Structures," *Front Robot AI,* vol. 6, p. 127, 2019, doi: 10.3389/frobt.2019.00127.

[83] H. Nesser and G. Lubineau, "Achieving Super Sensitivity in Capacitive Strain Sensing by Electrode Fragmentation," *ACS Appl Mater Interfaces,* vol. 13, no. 30, pp. 36062-36070, Aug 4 2021, doi: 10.1021/acsami.1c07704.

[84] J. Yuan, "Percolation of carbon nanomaterials for high-k polymer nanocomposites," *Chinese Chemical Letters,* vol. 28, no. 11, pp. 2036-2044, 2017, doi: 10.1016/j.cclet.2017.08.020.

[85] P.-J. Cao *et al.*, "A stretchable capacitive strain sensor having adjustable elastic modulus capability for wide‐range force detection," *Advanced Engineering Materials,* vol. 22, no. 3, p. 1901239, 2020.

[86] T. Dong, Y. Gu, T. Liu, and M. Pecht, "Resistive and capacitive strain sensors based on customized compliant electrode: Comparison and their wearable applications," *Sensors and Actuators A: Physical,* vol. 326, p. 112720, 2021.

[87] N. Zavanelli and W.-H. Yeo, "Advances in Screen Printing of Conductive Nanomaterials for Stretchable Electronics," *ACS Omega,* 2021, doi: 10.1021/acsomega.1c00638.

[88] A. P. Patnaik, S., "Fibres to Smart Textiles: Advances in Manufacturing, Technologies, and Applications," Chapter 17: Smart Textiles and Recent Developments, pp. 331-345, 2019.

[89] E. Messerschmitt, "Rheological Considerations for Screen Printing Inks," *Screen Print,* vol. 72, no. 10, pp. 62-65, 1982.

[90] N. Kapur, S. J. Abbott, E. D. Dolden, and P. H. Gaskell, "Predicting the behavior of screen printing," in *IEEE Trans. Compon. Packaging Manuf. Technol.* vol. 3, ed, 2013, pp. 508-515.

[91] S. J. Potts, C. Phillips, E. Jewell, B. Clifford, Y. C. Lau, and T. Claypole, "High-speed imaging the effect of snap-off distance and squeegee speed on the ink transfer mechanism of screen-printed carbon pastes," in *J. Coat. Technol. Res* vol. 17, ed: Springer US, 2020, pp. 447-459.

[92] C. Xu and N. Willenbacher, "How rheological properties affect fine-line screen printing of pastes: a combined rheological and high-speed video imaging study," in *J. Coat. Technol.* vol. 15, ed, 2018, pp. 1401-1412.

[93] S. Park *et al.*, "Fully Screen-Printed PI/PEG Blends Enabled Patternable Electrodes for Scalable Manufacturing of Skin-Conformal, Stretchable, Wearable Electronics," *ACS Appl Mater Interfaces,* vol. 15, no. 1, pp. 2092-2103, Jan 11 2023, doi: 10.1021/acsami.2c17653.

[94] I. A. Howard *et al.*, "Coated and Printed Perovskites for Photovoltaic Applications," *Adv Mater,* vol. 31, no. 26, p. e1806702, Jun 2019, doi: 10.1002/adma.201806702.

[95] O.-H. Huttunen, T. Happonen, J. Hiitola-Keinänen, P. Korhonen, J. Ollila, and J. Hiltunen, "Roll-To-Roll Screen-Printed Silver Conductors on a Polydimethyl Siloxane Substrate for Stretchable Electronics," *Industrial & Engineering Chemistry Research,* vol. 58, no. 43, pp. 19909-19916, 2019, doi: 10.1021/acs.iecr.9b03628.

[96] B. Philip, E. Jewell, P. Greenwood, and C. Weirman, "Material and process optimization screen printing carbon graphite pastes for mass production of heating elements," in *J. Manuf. Process* vol. 22, ed: The Society of Manufacturing Engineers, 2016, pp. 185-191.

[97] D. Riemer, "The Theoretical Fundamentals of the ScreenPrinting Process," *Microelectron. Int.,* vol. 6, no. 1, pp. 8-17, 1989.

[98] J. Liang, K. Tong, and Q. Pei, "A Water-Based Silver-Nanowire Screen-Print Ink for the Fabrication of Stretchable Conductors and Wearable Thin-Film Transistors," in *Adv. Mater.* vol. 28, ed: Wiley-VCH Verlag, 2016, pp. 5986-5996.

[99] W. J. Hyun, E. B. Secor, M. C. Hersam, C. D. Frisbie, and L. F. Francis, "High-resolution patterning of graphene by screen printing with a silicon stencil for highly flexible printed electronics," in *Adv. Mater.* vol. 27, ed, 2015, pp. 109-115.

[100] G. Grau, J. Cen, H. Kang, R. Kitsomboonloha, W. J. Scheideler, and V. Subramanian, "Gravure-printed electronics: recent progress in tooling development, understanding of printing physics, and realization of printed devices," *Flexible and Printed Electronics,* vol. 1, no. 2, 2016, doi: 10.1088/2058-8585/1/2/023002.

[101] M. Bariya *et al.*, "Roll-to-Roll Gravure Printed Electrochemical Sensors for Wearable and Medical Devices," *ACS Nano,* vol. 12, no. 7, pp. 6978-6987, Jul 24 2018, doi: 10.1021/acsnano.8b02505.

[102] H. A. D. Nguyen, C. Lee, K.-H. Shin, and D. Lee, "An Investigation of the Ink-Transfer Mechanism During the Printing Phase of High-Resolution Roll-to-Roll Gravure Printing," *IEEE Transactions on Components, Packaging and Manufacturing Technology,* vol. 5, no. 10, pp. 1516-1524, 2015, doi: 10.1109/tcpmt.2015.2473853.

[103] E. B. Secor, S. Lim, H. Zhang, C. D. Frisbie, L. F. Francis, and M. C. Hersam, "Gravure printing of graphene for large-area flexible electronics," *Adv Mater,* vol. 26, no. 26, pp. 4533-8, Jul 9 2014, doi: 10.1002/adma.201401052.

[104] J. Lee, J. Kim, Y. Noh, H. Jeong, and D. Lee, "Advanced technique for achieving 10-μm-width fine lines in roll-to-roll continuous gravure printing," *Precision Engineering,* vol. 69, pp. 1-7, 2021, doi: 10.1016/j.precisioneng.2021.01.001.

[105] W. J. Scheideler, J. Jang, M. A. Ul Karim, R. Kitsomboonloha, A. Zeumault, and V. Subramanian, "Gravure-Printed Sol-Gels on Flexible Glass: A Scalable Route to Additively Patterned Transparent Conductors," *ACS Appl Mater Interfaces,* vol. 7, no. 23, pp. 12679-87, Jun 17 2015, doi: 10.1021/acsami.5b00183.

[106] K. Kim, J. Kim, B. Kim, and S. Ko, "Fabrication of Microfluidic Structure Based Biosensor Using Roll-to-Roll Gravure Printing," *International Journal of Precision Engineering and Manufacturing-Green Technology,* vol. 5, no. 3, pp. 369-374, 2018, doi: 10.1007/s40684-018-0039-0.

[107] D. Sung, A. de la Fuente Vornbrock, and V. Subramanian, "Scaling and Optimization of Gravure-Printed Silver Nanoparticle Lines for Printed Electronics," *IEEE Transactions on Components and Packaging Technologies,* vol. 33, no. 1, pp. 105-114, 2010, doi: 10.1109/tcapt.2009.2021464.

[108] J. Park, J. Lee, S. Park, K.-H. Shin, and D. Lee, "Development of hybrid process for double-side flexible printed circuit boards using roll-to-roll gravure printing, via-hole printing, and electroless plating," *The International Journal of Advanced Manufacturing Technology,* vol. 82, no. 9-12, pp. 1921-1931, 2015, doi: 10.1007/s00170-015-7507-2.

[109] Q. Huang and Y. Zhu, "Printing Conductive Nanomaterials for Flexible and Stretchable Electronics: A Review of Materials, Processes, and Applications," *Advanced Materials Technologies,* vol. 4, no. 5, 2019, doi: 10.1002/admt.201800546.

[110] M. Singh, H. M. Haverinen, P. Dhagat, and G. E. Jabbour, "Inkjet printing-process and its applications," *Adv Mater,* vol. 22, no. 6, pp. 673-85, Feb 9 2010, doi: 10.1002/adma.200901141.

[111] G. K. S. Lau, M, "Ink-Jet Printing of Micro-Electro-Mechanical Systems (MEMS)," *Micromachines,* vol. 8, 6, p. 194, 2017.

[112] W. Wu, "Inorganic nanomaterials for printed electronics: a review," *Nanoscale,* vol. 9, no. 22, pp. 7342-7372, Jun 8 2017, doi: 10.1039/c7nr01604b.

[113] M. Gao, L. Li, and Y. Song, "Inkjet printing wearable electronic devices," *Journal of Materials Chemistry C,* vol. 5, no. 12, pp. 2971-2993, 2017, doi: 10.1039/c7tc00038c.

[114] J. Wiklund *et al.*, "A Review on Printed Electronics: Fabrication Methods, Inks, Substrates, Applications and Environmental Impacts," *Journal of Manufacturing and Materials Processing*, vol. 5, no. 3*,* doi: 10.3390/jmmp5030089.

[115] R. Tortorich and J.-W. Choi, "Inkjet Printing of Carbon Nanotubes," *Nanomaterials,* vol. 3, no. 3, pp. 453-468, 2013, doi: 10.3390/nano3030453.

[116] J. S. Jan de Gans, U., "Inkjet Printing of Well-Defined Polymer Dots and Arrays," *Langmuir,* vol. 20, pp. 7789-7793, 2004.

[117] H. B. S. Eral, D.; Duits, M.H.G; Mugele, F., "Suppressing the coffee stain effect: how to control colloidal self-assembly in evaporating drops using electrowetting," *Soft Matter,* vol. 7, 10, pp. 7090-7094, 2011.

[118] R. B. Deegan, O.; Dupont, T.; Huber, G.; Nagel, S.; Witten, T., "Capillary flow as the cause of ring stains from dried liquid drops," *Nature,* vol. 389, pp. 827-829, 1997.

[119] D. Bartolo, A. Boudaoud, G. Narcy, and D. Bonn, "Dynamics of non-Newtonian droplets," *Phys Rev Lett,* vol. 99, no. 17, p. 174502, Oct 26 2007, doi: 10.1103/PhysRevLett.99.174502.

[120] H. Wijshoff, "Drop dynamics in the inkjet printing process," *Current Opinion in Colloid & Interface Science,* vol. 36, pp. 20-27, 2018, doi: 10.1016/j.cocis.2017.11.004.

[121] L. Nayak, S. Mohanty, S. K. Nayak, and A. Ramadoss, "A review on inkjet printing of nanoparticle inks for flexible electronics," *Journal of Materials Chemistry C,* vol. 7, no. 29, pp. 8771-8795, 2019, doi: 10.1039/c9tc01630a.

[122] B. Derby, "Additive Manufacture of Ceramics Components by Inkjet Printing," *Engineering,* vol. 1, no. 1, pp. 113-123, 2015/03/01/ 2015, doi: https://doi.org/10.15302/J-ENG-2015014.

[123] L. Cai *et al.*, "Direct Printing for Additive Patterning of Silver Nanowires for Stretchable Sensor and Display Applications," *Advanced Materials Technologies,* vol. 3, no. 2, 2018, doi: 10.1002/admt.201700232.

[124] H. L. Hu, R., "Marangoni Effect Reverses Coffee-Ring Depositions," *J. Phys. Chem. B,* vol. 110, 14, pp. 7090-7094, 2006.

[125] M. Anyfantakis, Z. Geng, M. Morel, S. Rudiuk, and D. Baigl, "Modulation of the coffee-ring effect in particle/surfactant mixtures: the importance of particle-interface interactions," *Langmuir,* vol. 31, no. 14, pp. 4113-20, Apr 14 2015, doi: 10.1021/acs.langmuir.5b00453.

[126] N. D. Patil, P. G. Bange, R. Bhardwaj, and A. Sharma, "Effects of Substrate Heating and Wettability on Evaporation Dynamics and Deposition Patterns for a Sessile Water Droplet Containing Colloidal Particles," *Langmuir,* vol. 32, no. 45, pp. 11958-11972, Nov 15 2016, doi: 10.1021/acs.langmuir.6b02769.

[127] S. A. McBride, S. Dash, and K. K. Varanasi, "Evaporative Crystallization in Drops on Superhydrophobic and Liquid-Impregnated Surfaces," *Langmuir,* vol. 34, no. 41, pp. 12350-12358, Oct 16 2018, doi: 10.1021/acs.langmuir.8b00049.

[128] K. N. Al-Milaji, R. R. Secondo, T. N. Ng, N. Kinsey, and H. Zhao, "Interfacial Self-Assembly of Colloidal Nanoparticles in Dual-Droplet Inkjet Printing," *Advanced Materials Interfaces,* vol. 5, no. 10, 2018, doi: 10.1002/admi.201701561.

[129] R. P. Gandhiraman, V. Jayan, J. W. Han, B. Chen, J. E. Koehne, and M. Meyyappan, "Plasma jet printing of electronic materials on flexible and nonconformal objects," *ACS Appl Mater Interfaces,* vol. 6, no. 23, pp. 20860-7, Dec 10 2014, doi: 10.1021/am505325y.

[130] A. Mahajan, C. D. Frisbie, and L. F. Francis, "Optimization of aerosol jet printing for high-resolution, high-aspect ratio silver lines," *ACS Appl Mater Interfaces,* vol. 5, no. 11, pp. 4856-64, Jun 12 2013, doi: 10.1021/am400606y.

[131] M. E. Morales-Rodriguez, P. C. Joshi, J. R. Humphries, P. L. Fuhr, and T. J. McIntyre, "Fabrication of Low Cost Surface Acoustic Wave Sensors Using Direct Printing by Aerosol Inkjet," *IEEE Access,* vol. 6, pp. 20907-20915, 2018, doi: 10.1109/access.2018.2824118.

[132] C. Ou, A. L. Sangle, T. Chalklen, Q. Jing, V. Narayan, and S. Kar-Narayan, "Enhanced thermoelectric properties of flexible aerosol-jet printed carbon nanotube-based nanocomposites," *APL Materials,* vol. 6, no. 9, 2018, doi: 10.1063/1.5043547.

[133] T. Rahman, L. Renaud, D. Heo, M. Renn, and R. Panat, "Aerosol based direct-write micro-additive fabrication method for sub-mm 3D metal-dielectric structures," *Journal of Micromechanics and Microengineering,* vol. 25, no. 10, 2015, doi: 10.1088/0960-1317/25/10/107002.

[134] M. Smith, Y. S. Choi, C. Boughey, and S. Kar-Narayan, "Controlling and assessing the quality of aerosol jet printed features for large area and flexible electronics," *Flexible and Printed Electronics,* vol. 2, no. 1, 2017, doi: 10.1088/2058-8585/aa5af9.

[135] N. J. Wilkinson, M. A. A. Smith, R. W. Kay, and R. A. Harris, "A review of aerosol jet printing—a non-traditional hybrid process for micro-manufacturing," *The International Journal of Advanced Manufacturing Technology,* vol. 105, no. 11, pp. 4599-4619, 2019, doi: 10.1007/s00170-019-03438-2.

[136] J. Wiklund *et al.*, "A Review on Printed Electronics: Fabrication Methods, Inks, Substrates, Applications and Environmental Impacts," *Journal of Manufacturing and Materials Processing,* vol. 5, no. 3, 2021, doi: 10.3390/jmmp5030089.

[137] M. Saleh, C. Hu, and R. Panat, "Three-dimensional microarchitected materials and devices using nanoparticle assembly by pointwise spatial printing," *Sci. Adv.,* vol. 3, e160198, 2017.

[138] D. Zhao, T. Liu, J. G. Park, M. Zhang, J.-M. Chen, and B. Wang, "Conductivity enhancement of aerosol-jet printed electronics by using silver nanoparticles ink with carbon nanotubes," *Microelectronic Engineering,* vol. 96, pp. 71-75, 2012, doi: 10.1016/j.mee.2012.03.004.

[139] S. Agarwala *et al.*, "Wearable bandage-based strain sensor for home healthcare: Combining 3D aerosol jet printing and laser sintering," *ACS sensors,* vol. 4, no. 1, pp. 218-226, 2018.

[140] S. Agarwala, G. L. Goh, and W. Y. Yeong, "Aerosol Jet Printed Strain Sensor: Simulation Studies Analyzing the Effect of Dimension and Design on Performance (September 2018)," *IEEE Access,* vol. 6, pp. 63080-63086, 2018, doi: 10.1109/access.2018.2876647.

[141] Q. Jing, Y. S. Choi, M. Smith, C. Ou, T. Busolo, and S. Kar‐Narayan, "Freestanding Functional Structures by Aerosol‐Jet Printing for Stretchable Electronics and Sensing Applications," *Advanced Materials Technologies,* vol. 4, no. 7, p. 1900048, 2019.

[142] S.-H. Min *et al.*, "Stretchable chipless RFID multi-strain sensors using direct printing of aerosolised nanocomposite," *Sensors and Actuators A: Physical,* vol. 313, p. 112224, 2020.

[143] T. L. Phero, K. A. Novich, B. C. Johnson, M. D. McMurtrey, D. Estrada, and B. J. Jaques, "Additively manufactured strain sensors for in-pile applications," *Sensors and Actuators A: Physical,* vol. 344, p. 113691, 2022.

[144] N. Mkhize and H. Bhaskaran, "Electrohydrodynamic Jet Printing: Introductory Concepts and Considerations," *Small Science,* vol. 2, no. 2, 2021, doi: 10.1002/smsc.202100073.

[145] P. Richner, S. J. P. Kress, D. J. Norris, and D. Poulikakos, "Charge effects and nanoparticle pattern formation in electrohydrodynamic NanoDrip printing of colloids," *Nanoscale,* 10.1039/C5NR08783J vol. 8, no. 11, pp. 6028-6034, 2016, doi: 10.1039/C5NR08783J.

[146] B. Zhang, B. Seong, J. Lee, V. Nguyen, D. Cho, and D. Byun, "One-Step Sub-micrometer-Scale Electrohydrodynamic Inkjet Three-Dimensional Printing Technique with Spontaneous Nanoscale Joule Heating," *ACS Appl Mater Interfaces,* vol. 9, no. 35, pp. 29965-29972, Sep 6 2017, doi: 10.1021/acsami.7b08375.

[147] Y. Pan, Y. Huang, N. Bu, and Z. Yin, "Fabrication of Si-nozzles for parallel mechano-electrospinning direct writing," *Journal of Physics D: Applied Physics,* vol. 46, no. 25, 2013, doi: 10.1088/0022-3727/46/25/255301.

[148] Z. Cui, Y. Han, Q. Huang, J. Dong, and Y. Zhu, "Electrohydrodynamic printing of silver nanowires for flexible and stretchable electronics," *Nanoscale,* vol. 10, no. 15, pp. 6806-6811, 2018.

[149] Q. Huang and Y. Zhu, "Printed Electronics: Printing Conductive Nanomaterials for Flexible and Stretchable Electronics: A Review of Materials, Processes, and Applications (Adv. Mater. Technol. 5/2019)," *Advanced Materials Technologies,* vol. 4, no. 5, p. 1970029, 2019.

[150] M. S. Onses, E. Sutanto, P. M. Ferreira, A. G. Alleyne, and J. A. Rogers, "Mechanisms, capabilities, and applications of high‐resolution electrohydrodynamic jet printing," *Small,* vol. 11, no. 34, pp. 4237-4266, 2015.

[151] P. Ren and J. Dong, "Direct Fabrication of VIA Interconnects by Electrohydrodynamic Printing for Multi‐Layer 3D Flexible and Stretchable Electronics," *Advanced Materials Technologies,* vol. 6, no. 9, p. 2100280, 2021.

[152] P. Ren, Y. Liu, R. Song, B. O'Connor, J. Dong, and Y. Zhu, "Achieving high-resolution electrohydrodynamic printing of nanowires on elastomeric substrates through surface modification," *ACS Applied Electronic Materials,* vol. 3, no. 1, pp. 192-202, 2020.

[153] D. Wang *et al.*, "Electrohydrodynamic jet printing of PZT thick film micro-scale structures," *Journal of the European Ceramic Society,* vol. 35, no. 13, pp. 3475-3483, 2015.

[154] D. Wei, R. Zhang, M. N. Saadatzi, O. O. Olowo, and D. O. Popa, "Organic Piezoresistive Pressure Sensitive Robotic Skin for Physical Human-Robot Interaction," in *International Design Engineering Technical Conferences and Computers and Information in Engineering Conference*, 2020, vol. 83907: American Society of Mechanical Engineers, p. V001T01A013.

[155] S. K. Iravani, H.; Mirmohammadi, S.V.; Zolfaghari, B., "Synthesis of silver nanoparticles: chemical, physical and biological methods," *Res. Pharm. Sci.,* vol. 9, 6, pp. 385-406, 2014.

[156] G.-Y. Lee, M.-S. Kim, H.-S. Yoon, J. Yang, J.-B. Ihn, and S.-H. Ahn, "Direct printing of strain sensors via nanoparticle printer for the applications to composite structural health monitoring," *Procedia CIRP,* vol. 66, pp. 238-242, 2017.

[157] B. Niu, S. Yang, X. Tian, and T. Hua, "Highly sensitive and stretchable fiber strain sensors empowered by synergetic conductive network of silver nanoparticles and carbon nanotubes," *Applied Materials Today,* vol. 25, p. 101221, 2021.

[158] B. Radha, A. A. Sagade, and G. Kulkarni, "Flexible and semitransparent strain sensors based on micromolded Pd nanoparticle–carbon μ-stripes," *ACS applied materials & interfaces,* vol. 3, no. 7, pp. 2173-2178, 2011.

[159] W.-W. Jheng *et al.*, "Gold nanoparticle thin film-based strain sensors for monitoring human pulse," *ACS Applied Nano Materials,* vol. 4, no. 2, pp. 1712-1718, 2021.

[160] G.-Y. Lee *et al.*, "Highly sensitive solvent-free silver nanoparticle strain sensors with tunable sensitivity created using an aerodynamically focused nanoparticle printer," *ACS applied materials & interfaces,* vol. 11, no. 29, pp. 26421-26432, 2019.

[161] M. Segev-Bar and H. Haick, "Flexible Sensors Based on Nanoparticles," *ACS Nano,* vol. 7, no. 10, pp. 8366-8378, 2013/10/22 2013, doi: 10.1021/nn402728g.

[162] S. Y. Kim, B.; Miller, M.; Bowen, D.; Pines, D. J.; Daniels, K. M, "EGaIn-Silicone-Based Highly Stretchable and Flexible Strain Sensor for Real-Time Two Joint Robotic Motion Monitoring," *Sensors and Actuators A: Physical,* 342, p. 113659, 2022.

[163] S. Zhang *et al.*, "Highly stretchable, sensitive, and flexible strain sensors based on silver nanoparticles/carbon nanotubes composites," *Journal of Alloys and compounds,* vol. 652, pp. 48-54, 2015.

[164] X. Zhang *et al.*, "Flexible and high-performance piezoresistive strain sensors based on carbon nanoparticles@ polyurethane sponges," *Composites Science and Technology,* vol. 200, p. 108437, 2020.

[165] Z. Wang, X. Liang, T. Zhao, Y. Hu, P. Zhu, and R. Sun, "Facile synthesis of monodisperse silver nanoparticles for screen printing conductive inks," *Journal of Materials Science: Materials in Electronics,* vol. 28, no. 22, pp. 16939-16947, 2017, doi: 10.1007/s10854-017-7614-y.

[166] I. J. Fernandes *et al.*, "Silver nanoparticle conductive inks: synthesis, characterization, and fabrication of inkjet-printed flexible electrodes," *Sci Rep,* vol. 10, no. 1, p. 8878, Jun 1 2020, doi: 10.1038/s41598-020-65698-3.

[167] J. Perelaer and U. S. Schubert, "Novel approaches for low temperature sintering of inkjet-printed inorganic nanoparticles for roll-to-roll (R2R) applications," *Journal of Materials Research,* vol. 28, no. 4, pp. 564-573, 2013, doi: 10.1557/jmr.2012.419.

[168] S. G. Chen, Y.; Li, Y; Yan, X.; Ni, H.; Li, L., "A water-based silver nanowire ink for large-scale flexible transparent conductive films and touch screens," *J. Mater. Chem. C,* vol. 5, pp. 2404-2414, 2017.

[169] J. Liang, K. Tong, and Q. Pei, "A Water-Based Silver-Nanowire Screen-Print Ink for the Fabrication of Stretchable Conductors and Wearable Thin-Film Transistors," *Adv Mater,* vol. 28, no. 28, pp. 5986-96, Jul 2016, doi: 10.1002/adma.201600772.

[170] P. Zhang *et al.*, "Silver nanowires: Synthesis technologies, growth mechanism and multifunctional applications," *Materials Science and Engineering: B,* vol. 223, pp. 1-23, 2017, doi: 10.1016/j.mseb.2017.05.002.

[171] M. M. Ali *et al.*, "Printed strain sensor based on silver nanowire/silver flake composite on flexible and

stretchable TPU substrate," *Sensors and Actuators A: Physical,* vol. 274, pp. 109-115, 2018.

[172] S. Chen, Z. Lou, D. Chen, K. Jiang, and G. Shen, "Polymer‐enhanced highly stretchable conductive fiber strain sensor used for electronic data gloves," *Advanced Materials Technologies,* vol. 1, no. 7, p. 1600136, 2016.

[173] S. Han *et al.*, "Multiscale nanowire-microfluidic hybrid strain sensors with high sensitivity and stretchability," *npj Flexible Electronics,* vol. 2, no. 1, p. 16, 2018.

[174] K. H. Kim, N. S. Jang, S. H. Ha, J. H. Cho, and J. M. Kim, "Highly sensitive and stretchable resistive strain sensors based on microstructured metal nanowire/elastomer composite films," *Small,* vol. 14, no. 14, p. 1704232, 2018.

[175] K. K. Kim *et al.*, "Highly sensitive and stretchable multidimensional strain sensor with prestrained anisotropic metal nanowire percolation networks," *Nano letters,* vol. 15, no. 8, pp. 5240-5247, 2015.

[176] K. S. Kumar *et al.*, "Stretchable and sensitive silver nanowire-hydrogel strain sensors for proprioceptive actuation," *ACS applied materials & interfaces,* vol. 13, no. 31, pp. 37816-37829, 2021.

[177] T. Lee, W. Lee, S. W. Kim, J. J. Kim, and B. S. Kim, "Flexible textile strain wireless sensor functionalized with hybrid carbon nanomaterials supported ZnO nanowires with controlled aspect ratio," *Advanced Functional Materials,* vol. 26, no. 34, pp. 6206-6214, 2016.

[178] Q. Liao, M. Mohr, X. Zhang, Z. Zhang, Y. Zhang, and H.-J. Fecht, "Carbon fiber–ZnO nanowire hybrid structures for flexible and adaptable strain sensors," *Nanoscale,* vol. 5, no. 24, pp. 12350-12355, 2013.

[179] X. Xiao *et al.*, "High‐strain sensors based on ZnO nanowire/polystyrene hybridized flexible films," *Advanced materials,* vol. 23, no. 45, pp. 5440-5444, 2011.

[180] S. Yao, J. Yang, F. R. Poblete, X. Hu, and Y. Zhu, "Multifunctional electronic textiles using silver nanowire composites," *ACS applied materials & interfaces,* vol. 11, no. 34, pp. 31028-31037, 2019.

[181] W. Zhang, R. Zhu, V. Nguyen, and R. Yang, "Highly sensitive and flexible strain sensors based on vertical zinc oxide nanowire arrays," *Sensors and Actuators A: Physical,* vol. 205, pp. 164-169, 2014.

[182] K. N. Al-Milaji, Q. Huang, Z. Li, T. N. Ng, and H. Zhao, "Direct Embedment and Alignment of Silver Nanowires by Inkjet Printing for Stretchable Conductors," *ACS Applied Electronic Materials,* vol. 2, no. 10, pp. 3289-3298, 2020, doi: 10.1021/acsaelm.0c00616.

[183] A. T. S. Tilke, F.C.; Lorenz, H.; Blick, R.H.; Kotthaus, J.P., "2003," *Phys. Rev. B,* vol. 68, p. 075311, 2003.

[184] R. E. Triambulo, H.-G. Cheong, and J.-W. Park, "All-solution-processed foldable transparent electrodes of Ag nanowire mesh and metal matrix films for flexible electronics," *Organic Electronics,* vol. 15, no. 11, pp. 2685-2695, 2014, doi: 10.1016/j.orgel.2014.07.039.

[185] S. Hemmati, M. T. Harris, and D. P. Barkey, "Polyol Silver Nanowire Synthesis and the Outlook for a Green Process," *Journal of Nanomaterials,* vol. 2020, pp. 1-25, 2020, doi: 10.1155/2020/9341983.

[186] S. Coskun, B. Aksoy, and H. E. Unalan, "Polyol Synthesis of Silver Nanowires: An Extensive Parametric Study," *Crystal Growth & Design,* vol. 11, no. 11, pp. 4963-4969, 2011, doi: 10.1021/cg200874g.

[187] Y. M. Sun, B; Herricks, T. Xia, X., "Polyol Synthesis of Uniform Silver Nanowires: A Plausible Growth Mechanism and the Supporting Evidence," *Nano Letters,* vol. 3, no. 7, pp. 955–960, 2003.

[188] D. J. Finn, M. Lotya, and J. N. Coleman, "Inkjet printing of silver nanowire networks," *ACS Appl Mater Interfaces,* vol. 7, no. 17, pp. 9254-61, May 6 2015, doi: 10.1021/acsami.5b01875.

[189] K. Chen *et al.*, "Printed Carbon Nanotube Electronics and Sensor Systems," *Adv Mater,* vol. 28, no. 22, pp. 4397-414, Jun 2016, doi: 10.1002/adma.201504958.

[190] Y. Gao, X. Fang, J. Tan, T. Lu, L. Pan, and F. Xuan, "Highly sensitive strain sensors based on fragmentized carbon nanotube/polydimethylsiloxane composites," *Nanotechnology,* vol. 29, no. 23, p. 235501, 2018.

[191] Y. He *et al.*, "Wearable strain sensors based on a porous polydimethylsiloxane hybrid with carbon nanotubes and graphene," *ACS Applied Materials & Interfaces,* vol. 13, no. 13, pp. 15572-15583, 2021.

[192] T. N. Lam *et al.*, "Microfluidic preparation of highly stretchable natural rubber microfiber containing CNT/PEDOT: PSS hybrid for fabric-sewable wearable strain sensor," *Composites Science and Technology,* vol. 210, p. 108811, 2021.

[193] H. J. Lee *et al.*, "An electronically perceptive bioinspired soft wet-adhesion actuator with carbon nanotube-based strain sensors," *ACS nano,* vol. 15, no. 9, pp. 14137-14148, 2021.

[194] B. Liang *et al.*, "Ultra-stretchable and highly sensitive strain sensor based on gradient structure carbon nanotubes," *Nanoscale,* vol. 10, no. 28, pp. 13599-13606, 2018.

[195] W. Lin *et al.*, "Simultaneously achieving ultrahigh sensitivity and wide detection range for stretchable strain sensors with an interface‐locking strategy," *Advanced Materials Technologies,* vol. 5, no. 5, p. 2000008, 2020.

[196] L. Ling, F. Liu, J. Li, G. Zhang, R. Sun, and C. P. Wong, "Self‐Healable and Mechanically Reinforced Multidimensional‐Carbon/Polyurethane Dielectric Nanocomposite Incorporates Various Functionalities for Capacitive Strain Sensor Applications,"

Macromolecular Chemistry and Physics, vol. 219, no. 23, p. 1800369, 2018.

[197] L. Liu *et al.*, "Highly stretchable, sensitive and wide linear responsive fabric-based strain sensors with a self-segregated carbon nanotube (CNT)/Polydimethylsiloxane (PDMS) coating," *Progress in Natural Science: Materials International,* vol. 32, no. 1, pp. 34-42, 2022.

[198] X. Liu *et al.*, "Densely packed, highly strain sensitive carbon nanotube composites with sufficient polymer penetration," ed: Elsevier, 2020.

[199] S. Ryu *et al.*, "Extremely elastic wearable carbon nanotube fiber strain sensor for monitoring of human motion," *ACS nano,* vol. 9, no. 6, pp. 5929-5936, 2015.

[200] H. A. Toprakci, S. K. Kalanadhabhatla, R. J. Spontak, and T. K. Ghosh, "Polymer nanocomposites containing carbon nanofibers as soft printable sensors exhibiting strain‐reversible piezoresistivity," *Advanced Functional Materials,* vol. 23, no. 44, pp. 5536-5542, 2013.

[201] L. Wang *et al.*, "Highly stretchable, anti-corrosive and wearable strain sensors based on the PDMS/CNTs decorated elastomer nanofiber composite," *Chemical Engineering Journal,* vol. 362, pp. 89-98, 2019.

[202] S. Wang *et al.*, "Network cracks-based wearable strain sensors for subtle and large strain detection of human motions," *Journal of Materials Chemistry C,* vol. 6, no. 19, pp. 5140-5147, 2018.

[203] X. Wang *et al.*, "A highly stretchable carbon nanotubes/thermoplastic polyurethane fiber-shaped strain sensor with porous structure for human motion monitoring," *Composites Science and Technology,* vol. 168, pp. 126-132, 2018.

[204] T. Xiao, C. Qian, R. Yin, K. Wang, Y. Gao, and F. Xuan, "3D printing of flexible strain sensor array based on UV‐curable multiwalled carbon nanotube/elastomer composite," *Advanced Materials Technologies,* vol. 6, no. 1, p. 2000745, 2021.

[205] H. Xue and J. Hu, "A liquid power-ultrasound based green fabrication process for flexible strain sensors at room temperature and normal pressure," *Sensors and Actuators A: Physical,* vol. 329, p. 112822, 2021.

[206] Y. Yu *et al.*, "Flexible and transparent strain sensors based on super-aligned carbon nanotube films," *Nanoscale,* vol. 9, no. 20, pp. 6716-6723, 2017.

[207] Z. Zeng, B. Hao, D. Li, D. Cheng, G. Cai, and X. Wang, "Large-scale production of weavable, dyeable and durable spandex/CNT/cotton core-sheath yarn for wearable strain sensors," *Composites Part A: Applied Science and Manufacturing,* vol. 149, p. 106520, 2021.

[208] Y. Zheng *et al.*, "A highly stretchable and stable strain sensor based on hybrid carbon nanofillers/polydimethylsiloxane conductive composites for large human motions monitoring," *Composites Science and Technology,* vol. 156, pp. 276-286, 2018.

[209] S. Kholghi Eshkalak, A. Chinnappan, W. A. D. M. Jayathilaka, M. Khatibzadeh, E. Kowsari, and S. Ramakrishna, "A review on inkjet printing of CNT composites for smart applications," *Applied Materials Today,* vol. 9, pp. 372-386, 2017, doi: 10.1016/j.apmt.2017.09.003.

[210] Z. P. Huang, J. W. Xu, Z. F. Ren, J. H. Wang, M. P. Siegal, and P. N. Provencio, "Growth of highly oriented carbon nanotubes by plasma-enhanced hot filament chemical vapor deposition," *Applied Physics Letters,* vol. 73, no. 26, pp. 3845-3847, 1998, doi: 10.1063/1.122912.

[211] L. Boumia, M. Zidour, A. Benzair, and A. Tounsi, "A Timoshenko beam model for vibration analysis of chiral single-walled carbon nanotubes," *Physica E: Low-dimensional Systems and Nanostructures,* vol. 59, pp. 186-191, 2014, doi: 10.1016/j.physe.2014.01.020.

[212] R. P. Tortorich and J. W. Choi, "Inkjet Printing of Carbon Nanotubes," *Nanomaterials (Basel),* vol. 3, no. 3, pp. 453-468, Jul 29 2013, doi: 10.3390/nano3030453.

[213] N. Gupta, S. M. Gupta, and S. K. Sharma, "Carbon nanotubes: synthesis, properties and engineering applications," *Carbon Letters,* vol. 29, no. 5, pp. 419-447, 2019, doi: 10.1007/s42823-019-00068-2.

[214] O. Zaytseva and G. Neumann, "Carbon nanomaterials: production, impact on plant development, agricultural and environmental applications," *Chemical and Biological Technologies in Agriculture,* vol. 3, no. 1, 2016, doi: 10.1186/s40538-016-0070-8.

[215] Y. Shi, L. Ren, D. Li, H. Gao, and B. Yang, "Optimization Conditions for Single-Walled Carbon Nanotubes Dispersion," *Journal of Surface Engineered Materials and Advanced Technology,* vol. 03, no. 01, pp. 6-12, 2013, doi: 10.4236/jsemat.2013.31002.

[216] W. H. Duan, Q. Wang, and F. Collins, "Dispersion of carbon nanotubes with SDS surfactants: a study from a binding energy perspective," *Chemical Science,* 10.1039/C0SC00616E vol. 2, no. 7, pp. 1407-1413, 2011, doi: 10.1039/C0SC00616E.

[217] K. E. Whitener and P. E. Sheehan, "Graphene synthesis," *Diamond and Related Materials,* vol. 46, pp. 25-34, 2014, doi: 10.1016/j.diamond.2014.04.006.

[218] P. He *et al.*, "Screen-Printing of a Highly Conductive Graphene Ink for Flexible Printed Electronics," *ACS Appl Mater Interfaces,* vol. 11, no. 35, pp. 32225-32234, Sep 4 2019, doi: 10.1021/acsami.9b04589.

[219] J. Li, F. Ye, S. Vaziri, M. Muhammed, M. C. Lemme, and M. Ostling, "Efficient inkjet printing of

graphene," *Adv Mater,* vol. 25, no. 29, pp. 3985-92, Aug 7 2013, doi: 10.1002/adma.201300361.

[220] Z. Duan, Z. Yuan, Y. Jiang, L. Yuan, and H. Tai, "Amorphous carbon material of daily carbon ink: emerging applications in pressure, strain, and humidity sensors," *Journal of Materials Chemistry C,* 2023, doi: 10.1039/d3tc00016h.

[221] S. Khodabakhshi, P. F. Fulvio, and E. Andreoli, "Carbon black reborn: Structure and chemistry for renewable energy harnessing," *Carbon,* vol. 162, pp. 604-649, 2020, doi: 10.1016/j.carbon.2020.02.058.

[222] F. Arduini, S. Cinti, V. Mazzaracchio, V. Scognamiglio, A. Amine, and D. Moscone, "Carbon black as an outstanding and affordable nanomaterial for electrochemical (bio)sensor design," *Biosens Bioelectron,* vol. 156, p. 112033, May 15 2020, doi: 10.1016/j.bios.2020.112033.

[223] Q. Li, S. Luo, Y. Wang, and Q.-M. Wang, "Carbon based polyimide nanocomposites thin film strain sensors fabricated by ink-jet printing method," *Sensors and Actuators A: Physical,* vol. 300, p. 111664, 2019.

[224] X. Chen *et al.*, "A Single-material-printed, Low-cost design for a Carbon-based fabric strain sensor," *Materials & Design,* vol. 221, p. 110926, 2022.

[225] X. Guo *et al.*, "Highly stretchable strain sensor based on SWCNTs/CB synergistic conductive network for wearable human-activity monitoring and recognition," *Smart Materials and Structures,* vol. 26, no. 9, p. 095017, 2017.

[226] R. Li, K. Dong, M. Panahi-Sarmad, S. Li, and X. Xiao, "Three-dimensional printing of a flexible capacitive pressure sensor array in the assembly network of carbon fiber electrodes and interlayer of a porous polyurethane dielectric," *ACS Applied Electronic Materials,* vol. 3, no. 9, pp. 3999-4008, 2021.

[227] D. Zymelka, K. Togashi, and T. Kobayashi, "Carbon-based printed strain sensor array for remote and automated structural health monitoring," *Smart Materials and Structures,* vol. 29, no. 10, p. 105022, 2020.

[228] W. Zhang, A. A. Dehghani-Sanij, and R. S. Blackburn, "Carbon based conductive polymer composites," *Journal of Materials Science,* vol. 42, no. 10, pp. 3408-3418, 2007/05/01 2007, doi: 10.1007/s10853-007-1688-5.

[229] S. Zips *et al.*, "Fully Printed μ-Needle Electrode Array from Conductive Polymer Ink for Bioelectronic Applications," *ACS Applied Materials & Interfaces,* vol. 11, no. 36, pp. 32778-32786, 2019/09/11 2019, doi: 10.1021/acsami.9b11774.

[230] H. Liu *et al.*, "Electrically conductive polymer composites for smart flexible strain sensors: a critical review," *Journal of Materials Chemistry C,* 10.1039/C8TC04079F vol. 6, no. 45, pp. 12121-12141, 2018, doi: 10.1039/C8TC04079F.

[231] R. Madhavan, "Flexible and stretchable strain sensors fabricated by inkjet printing of silver nanowire-ecoflex composites," *Journal of Materials Science: Materials in Electronics,* vol. 33, no. 7, pp. 3465-3484, 2022/03/01 2022, doi: 10.1007/s10854-021-07540-8.

[232] X. Wu, Y. Han, X. Zhang, and C. Lu, "Highly Sensitive, Stretchable, and Wash-Durable Strain Sensor Based on Ultrathin Conductive Layer@Polyurethane Yarn for Tiny Motion Monitoring," *ACS Applied Materials & Interfaces,* vol. 8, no. 15, pp. 9936-9945, 2016/04/20 2016, doi: 10.1021/acsami.6b01174.

[233] M. Wang *et al.*, "Enhanced electrical conductivity and piezoresistive sensing in multi-wall carbon nanotubes/polydimethylsiloxane nanocomposites via the construction of a self-segregated structure," *Nanoscale,* 10.1039/C7NR02322G vol. 9, no. 31, pp. 11017-11026, 2017, doi: 10.1039/C7NR02322G.

[234] J. D. Pegan *et al.*, "Skin-mountable stretch sensor for wearable health monitoring," *Nanoscale,* 10.1039/C6NR04467K vol. 8, no. 39, pp. 17295-17303, 2016, doi: 10.1039/C6NR04467K.

[235] S.-J. Park, J. Kim, M. Chu, and M. Khine, "Highly Flexible Wrinkled Carbon Nanotube Thin Film Strain Sensor to Monitor Human Movement," *Advanced Materials Technologies,* https://doi.org/10.1002/admt.201600053 vol. 1, no. 5, p. 1600053, 2016/08/01 2016, doi: https://doi.org/10.1002/admt.201600053.

[236] M. Somvanshi, P. Chavan, S. Tambade, and S. Shinde, "A review of machine learning techniques using decision tree and support vector machine," in *2016 international conference on computing communication control and automation (ICCUBEA)*, 2016: IEEE, pp. 1-7.

[237] W. S. Noble, "What is a support vector machine?," *Nature biotechnology,* vol. 24, no. 12, pp. 1565-1567, 2006.

[238] A. Tharwat, T. Gaber, A. Ibrahim, and A. E. Hassanien, "Linear discriminant analysis: A detailed tutorial," *AI communications,* vol. 30, no. 2, pp. 169-190, 2017.

[239] P. Xanthopoulos, P. M. Pardalos, T. B. Trafalis, P. Xanthopoulos, P. M. Pardalos, and T. B. Trafalis, "Linear discriminant analysis," *Robust data mining,* pp. 27-33, 2013.

[240] M. S. Crouse, R. D. Nowak, and R. G. Baraniuk, "Wavelet-based statistical signal processing using hidden Markov models," *IEEE Transactions on signal processing,* vol. 46, no. 4, pp. 886-902, 1998.

[241] X. Liang, R. Ghannam, and H. Heidari, "Wrist-worn gesture sensing with wearable intelligence," *IEEE Sensors Journal,* vol. 19, no. 3, pp. 1082-1090, 2018.

[242] A. Ferrone *et al.*, "Wearable band for hand gesture recognition based on strain sensors," in *2016 6th IEEE International Conference on Biomedical Robotics and Biomechatronics (BioRob)*, 2016: IEEE, pp. 1319-1322.

[243] P. B. Shull, S. Jiang, Y. Zhu, and X. Zhu, "Hand gesture recognition and finger angle estimation via wrist-worn modified barometric pressure sensing," *IEEE Transactions on Neural Systems and Rehabilitation Engineering,* vol. 27, no. 4, pp. 724-732, 2019.

[244] Y. Zhang, Y. Huang, Y. Ge, and N. Bao, "A master–slave hand operation cooperative perception system for grasping object via information fusion of flexible strain sensors," *Measurement,* vol. 169, p. 108437, 2021.

[245] A. Aldahiri, B. Alrashed, and W. Hussain, "Trends in using IoT with machine learning in health prediction system," *Forecasting,* vol. 3, no. 1, pp. 181-206, 2021.

[246] N. Zavanelli, "Wavelet Analysis for Time Series Financial Signals via Element Analysis," *ArXiv,* p. arXiv:2301.13255, 2023.

[247] X. Zhao, N. Evans, and J.-L. Dugelay, "A subspace co-training framework for multi-view clustering," *Pattern Recognition Letters,* vol. 41, pp. 73-82, 2014.

[248] O. Dehzangi, M. Taherisadr, and R. ChangalVala, "IMU-based gait recognition using convolutional neural networks and multi-sensor fusion," *Sensors,* vol. 17, no. 12, p. 2735, 2017.

[249] S. Bhattacharyya, A. Konar, and D. Tibarewala, "Motor imagery, P300 and error-related EEG-based robot arm movement control for rehabilitation purpose," *Medical & biological engineering & computing,* vol. 52, pp. 1007-1017, 2014.

[250] M. Ringnér, "What is principal component analysis?," *Nature biotechnology,* vol. 26, no. 3, pp. 303-304, 2008.

[251] R. Bro and A. K. Smilde, "Principal component analysis," *Analytical methods,* vol. 6, no. 9, pp. 2812-2831, 2014.

[252] W. Zhu, Z. T. Webb, K. Mao, and J. Romagnoli, "A deep learning approach for process data visualization using t-distributed stochastic neighbor embedding," *Industrial & Engineering Chemistry Research,* vol. 58, no. 22, pp. 9564-9575, 2019.

[253] J. Soni, N. Prabakar, and H. Upadhyay, "Visualizing high-dimensional data using t-distributed stochastic neighbor embedding algorithm," *Principles of data science,* pp. 189-206, 2020.

[254] X. Guo *et al.*, "Biomimetic flexible strain sensor with high linearity using double conducting layers," *Composites Science and Technology,* vol. 213, p. 108908, 2021.

[255] X. Wu, X. Luo, Z. Song, Y. Bai, B. Zhang, and G. Zhang, "Ultra‐Robust and Sensitive Flexible Strain Sensor for Real‐Time and Wearable Sign Language Translation," *Advanced Functional Materials,* p. 2303504, 2023.

[256] D. Liu, T. Guo, and M. Chen, "Fault Detection Based on Modified t-SNE," in *2019 CAA Symposium on Fault Detection, Supervision and Safety for Technical Processes (SAFEPROCESS)*, 2019: IEEE, pp. 269-273.

[257] P. Lv *et al.*, "Ultrathin encapsulated rGO strain sensor for gesture recognition," *Microelectronic Engineering,* vol. 259, p. 111779, 2022.

[258] S. Karamizadeh, S. M. Abdullah, A. A. Manaf, M. Zamani, and A. Hooman, "An overview of principal component analysis," *Journal of Signal and Information Processing,* vol. 4, no. 3B, p. 173, 2013.

[259] L. Van der Maaten and G. Hinton, "Visualizing data using t-SNE," *Journal of machine learning research,* vol. 9, no. 11, 2008.

[260] S. Albawi, T. A. Mohammed, and S. Al-Zawi, "Understanding of a convolutional neural network," in *2017 international conference on engineering and technology (ICET)*, 2017: Ieee, pp. 1-6.

[261] Z. Li, F. Liu, W. Yang, S. Peng, and J. Zhou, "A survey of convolutional neural networks: analysis, applications, and prospects," *IEEE transactions on neural networks and learning systems,* 2021.

[262] P. Kim and P. Kim, "Convolutional neural network," *MATLAB deep learning: with machine learning, neural networks and artificial intelligence,* pp. 121-147, 2017.

[263] L. Jin *et al.*, "Flexible unimodal strain sensors for human motion detection and differentiation," *npj Flexible Electronics,* vol. 6, no. 1, p. 74, 2022.

[264] L. Jiao, H. Wu, R. Bie, A. Umek, and A. Kos, "Multi-sensor golf swing classification using deep CNN," *Procedia Computer Science,* vol. 129, pp. 59-65, 2018.

[265] Z. Liu *et al.*, "A highly sensitive stretchable strain sensor based on multi-functionalized fabric for respiration monitoring and identification," *Chemical Engineering Journal,* vol. 426, p. 130869, 2021.

[266] M. Shaha and M. Pawar, "Transfer learning for image classification," in *2018 second international conference on electronics, communication and aerospace technology (ICECA)*, 2018: IEEE, pp. 656-660.

[267] Q. Hu, X. Tang, and W. Tang, "A real-time patient-specific sleeping posture recognition system using pressure sensitive conductive sheet and transfer learning," *IEEE Sensors Journal,* vol. 21, no. 5, pp. 6869-6879, 2020.

[268] C. Tan, F. Sun, T. Kong, W. Zhang, C. Yang, and C. Liu, "A survey on deep transfer learning," in *Artificial Neural Networks and Machine Learning–ICANN 2018: 27th International Conference on Artificial Neural Networks, Rhodes, Greece, October 4-7, 2018, Proceedings, Part III 27*, 2018: Springer, pp. 270-279.

[269] Z. C. Lipton, J. Berkowitz, and C. Elkan, "A critical review of recurrent neural networks for sequence learning," *arXiv preprint arXiv:1506.00019,* 2015.

[270] S. Hochreiter and J. Schmidhuber, "Long short-term memory," *Neural computation,* vol. 9, no. 8, pp. 1735-1780, 1997.

[271] J. Chung, C. Gulcehre, K. Cho, and Y. Bengio, "Empirical evaluation of gated recurrent neural networks on sequence modeling," *arXiv preprint arXiv:1412.3555,* 2014.

[272] X. A. Nguyen, S. Gong, W. Cheng, and S. Chauhan, "A stretchable gold nanowire sensor and its characterization using machine learning for motion tracking," *IEEE Sensors Journal,* vol. 21, no. 13, pp. 15269-15276, 2021.

[273] D. Kim, M. Kim, J. Kwon, Y.-L. Park, and S. Jo, "Semi-supervised gait generation with two microfluidic soft sensors," *IEEE Robotics and Automation Letters,* vol. 4, no. 3, pp. 2501-2507, 2019.

[274] T. G. Thuruthel, K. Gilday, and F. Iida, "Drift-free latent space representation for soft strain sensors," in *2020 3rd IEEE International Conference on Soft Robotics (RoboSoft)*, 2020: IEEE, pp. 138-143.

[275] H. Park, J. Cho, J. Park, Y. Na, and J. Kim, "Sim-to-real transfer learning approach for tracking multi-DOF ankle motions using soft strain sensors," *IEEE Robotics and Automation Letters,* vol. 5, no. 2, pp. 3525-3532, 2020.

[276] J. Slemenšek *et al.*, "Human Gait Activity Recognition Machine Learning Methods," *Sensors,* vol. 23, no. 2, p. 745, 2023.

[277] Q. Lin *et al.*, "E-jacket: posture detection with loose-fitting garment using a novel strain sensor," in *2020 19th ACM/IEEE International Conference on Information Processing in Sensor Networks (IPSN)*, 2020: IEEE, pp. 49-60.

[278] Y. Li *et al.*, "Low‐Cost Data Glove Based on Deep‐Learning‐Enhanced Flexible Multiwalled Carbon Nanotube Sensors for Real‐Time Gesture Recognition," *Advanced Intelligent Systems,* p. 2200128, 2022.

[279] Y. Qiu *et al.*, "Nondestructive identification of softness via bioinspired multisensory electronic skins integrated on a robotic hand," *npj Flexible Electronics,* vol. 6, no. 1, p. 45, 2022.

[280] V. Sze, Y.-H. Chen, J. Emer, A. Suleiman, and Z. Zhang, "Hardware for machine learning: Challenges and opportunities," in *2017 IEEE Custom Integrated Circuits Conference (CICC)*, 2017: IEEE, pp. 1-8.

[281] V. Sze, "Designing hardware for machine learning: The important role played by circuit designers," *IEEE Solid-State Circuits Magazine,* vol. 9, no. 4, pp. 46-54, 2017.

[282] R. Mina, C. Jabbour, and G. E. Sakr, "A review of machine learning techniques in analog integrated circuit design automation," *Electronics,* vol. 11, no. 3, p. 435, 2022.

[283] K. T. Lee, P. S. Chee, E. H. Lim, and C. C. Lim, "Artificial intelligence (AI)-driven smart glove for object recognition application," *Materials Today: Proceedings,* vol. 64, pp. 1563-1568, 2022.

[284] Y. Zhang *et al.*, "Real-time sitting behavior tracking and analysis for rectification of sitting habits by strain sensor-based flexible data bands," *Measurement Science and Technology,* vol. 31, no. 5, p. 055102, 2020.

[285] Y. Ma *et al.*, "Flexible all-textile dual tactile-tension sensors for monitoring athletic motion during taekwondo," *Nano Energy,* vol. 85, p. 105941, 2021.

[286] Y. Jin *et al.*, "Soft sensing shirt for shoulder kinematics estimation," in *2020 IEEE International Conference on Robotics and Automation (ICRA)*, 2020: IEEE, pp. 4863-4869.

[287] L. Lin *et al.*, "Superhydrophobic and wearable TPU based nanofiber strain sensor with outstanding sensitivity for high-quality body motion monitoring," *Chemical Engineering Journal,* vol. 419, p. 129513, 2021.

[288] Y. Mengüç *et al.*, "Soft wearable motion sensing suit for lower limb biomechanics measurements," in *2013 IEEE International Conference on Robotics and Automation*, 2013: IEEE, pp. 5309-5316.

[289] Y. Gao, S. Gu, F. Jia, and G. Gao, "A skin-matchable, recyclable and biofriendly strain sensor based on a hydrolyzed keratin-containing hydrogel," *Journal of Materials Chemistry A,* vol. 8, no. 45, pp. 24175-24183, 2020.

[290] T. Alam, F. Saidane, A. Al Faisal, A. Khan, and G. Hossain, "Smart-textile strain sensor for human joint monitoring," *Sensors and Actuators A: Physical,* vol. 341, p. 113587, 2022.

[291] H. Wang, D. Li, W. Zhong, L. Xu, T. Jiang, and Z. L. Wang, "Self-powered inhomogeneous strain sensor enabled joint motion and three-dimensional muscle sensing," *ACS applied materials & interfaces,* vol. 11, no. 37, pp. 34251-34257, 2019.

[292] H. Nakamoto, H. Ootaka, M. Tada, I. Hirata, F. Kobayashi, and F. Kojima, "Stretchable strain sensor with anisotropy and application for joint angle measurement," *IEEE Sensors Journal,* vol. 16, no. 10, pp. 3572-3579, 2016.

[293] Z. Yang *et al.*, "Graphene textile strain sensor with negative resistance variation for human motion

detection," *ACS nano,* vol. 12, no. 9, pp. 9134-9141, 2018.

[294] H. Jeon, S. K. Hong, M. S. Kim, S. J. Cho, and G. Lim, "Omni-purpose stretchable strain sensor based on a highly dense nanocracking structure for whole-body motion monitoring," *ACS applied materials & interfaces,* vol. 9, no. 48, pp. 41712-41721, 2017.

[295] J.-B. Chossat, Y. Tao, V. Duchaine, and Y.-L. Park, "Wearable soft artificial skin for hand motion detection with embedded microfluidic strain sensing," in *2015 IEEE international conference on robotics and automation (ICRA)*, 2015: IEEE, pp. 2568-2573.

[296] Y.-F. Yang *et al.*, "An ultrasensitive strain sensor with a wide strain range based on graphene armour scales," *Nanoscale,* vol. 10, no. 24, pp. 11524-11530, 2018.

[297] S. Lee, D. Jo, K.-B. Kim, J. Jang, and W. Park, "Wearable sign language translation system using strain sensors," *Sensors and Actuators A: Physical,* vol. 331, p. 113010, 2021.

[298] X. Yu *et al.*, "Skin-integrated wireless haptic interfaces for virtual and augmented reality," *Nature,* vol. 575, no. 7783, pp. 473-479, 2019.

[299] Z. Zhou *et al.*, "Sign-to-speech translation using machine-learning-assisted stretchable sensor arrays," *Nature Electronics,* vol. 3, no. 9, pp. 571-578, 2020.

[300] T. Yan *et al.*, "Highly sensitive detection of subtle movement using a flexible strain sensor from helically wrapped carbon yarns," *Journal of Materials Chemistry C,* vol. 7, no. 32, pp. 10049-10058, 2019.

[301] M. Su *et al.*, "Nanoparticle based curve arrays for multirecognition flexible electronics," *Advanced Materials,* vol. 28, no. 7, pp. 1369-1374, 2016.

[302] Y. Wang *et al.*, "A durable nanomesh on-skin strain gauge for natural skin motion monitoring with minimum mechanical constraints," *Science advances,* vol. 6, no. 33, p. eabb7043, 2020.

[303] S. W. Lee *et al.*, "Enhanced sensitivity of patterned graphene strain sensors used for monitoring subtle human body motions," *ACS applied materials & interfaces,* vol. 9, no. 12, pp. 11176-11183, 2017.